CHEMICAL VAPOR DEPOSITION OF MULTISPECTRAL DOMES

B. A. diBenedetto, et al

Raytheon Company

Prepared for:

Air Force Materials Laboratory

April 1975

AFML-TR-75-27

CHEMICAL VAPOR DEPOSITION OF MULTISPECTRAL DOMES

RAYTHEON COMPANY
RESEARCH DIVISION
WALTHAM, MASSACHUSETTS

APRIL 1975

FINAL REPORT FOR PERIOD MARCH 1973 — SEPTEMBER 1974

Approved for public release; distribution unlimited.

AIR FORCE MATERIALS LABORATORY
AIR FORCE SYSTEMS COMMAND
WRIGHT–PATTERSON AIR FORCE BASE, OHIO 45433

UNCLASSIFIED

SECURITY CLASSIFICATION OF THIS PAGE (When Data Entered)

REPORT DOCUMENTATION PAGE		READ INSTRUCTIONS BEFORE COMPLETING FORM
1. REPORT NUMBER AFML-TR-75-27	2. GOVT ACCESSION NO.	3. RECIPIENT'S CATALOG NUMBER
4. TITLE (and Subtitle) CHEMICAL VAPOR DEPOSITION OF MULTISPECTRAL DOMES		5. TYPE OF REPORT & PERIOD COVERED Final Report - 19 March 1973 to 19 September 1974 6. PERFORMING ORG. REPORT NUMBER S-1792
7. AUTHOR(s) B. A. diBenedetto J. Pappis		8. CONTRACT OR GRANT NUMBER(s) F33615-73-C-1073
9. PERFORMING ORGANIZATION NAME AND ADDRESS Raytheon Company Research Division Waltham, MA 02154		10. PROGRAM ELEMENT, PROJECT, TASK AREA & WORK UNIT NUMBERS Project No. 7371 Task No: 737101
11. CONTROLLING OFFICE NAME AND ADDRESS Air Force Materials Laboratory (LPO) Air Force Systems Command Wright-Patterson AFB, Ohio 45433		12. REPORT DATE April 1975 13. NUMBER OF PAGES 89
14. MONITORING AGENCY NAME & ADDRESS (if different from Controlling Office)		15. SECURITY CLASS. (of this report) Unclassified 15a. DECLASSIFICATION/DOWNGRADING SCHEDULE

16. DISTRIBUTION STATEMENT (of this Report)

Approved for public release; distribution unlimited.

17. DISTRIBUTION STATEMENT (of the abstract entered in Block 20, if different from Report)

18. SUPPLEMENTARY NOTES

19. KEY WORDS (Continue on reverse side if necessary and identify by block number)

Reconnaissance
Chemical Vapor Deposition
Zinc sulfide
Zinc sulfo-selenide
Multispectral
FLIR

20. ABSTRACT (Continue on reverse side if necessary and identify by block number)

The significance of this development program to the Air Force is the demonstrated capability of fabricating chemical vapor deposited zinc sulfide windows and hemispherical domes. A zinc sulfide plate, 10 × 10 × 5/8 in., and a 9-inch hemispherical dome were fabricated and optically polished to specification. As a result of this work the optical and structural properties of zinc sulfide were significantly improved. For example, a 60 percent increase in strength was realized. It was also demonstrated that it is possible using the CVD process to deposit multiple domes per run. With further

DD FORM 1 JAN 73 1473 EDITION OF 1 NOV 65 IS OBSOLETE

UNCLASSIFIED

SECURITY CLASSIFICATION OF THIS PAGE (When Data Entered)

development a significant cost savings for this type of hardware should be realized.

Significant progress was also made in the development of zinc sulfo-selenide solid solutions. Improvements were realized in the optical and structural properties of these deposits. At the conclusion of the program a clearer understanding of the cause of scatter in these materials and zinc sulfide had been attained that resulted in improved materials.

NOTICE

When Government drawings, specifications, or other data are used for any purpose other than in connection with a definitely related Government procurement operation, the United States Government thereby incurs no responsibility nor any obligation whatsoever; and the fact that the government may have formulated, furnished, or in any way supplied the said drawings, specifications, or other data, is not to be regarded by implication or otherwise as in any manner licensing the holder or any other person or corporation, or conveying any rights or permission to manufacture, use, or sell any patented invention that may in any way be related thereto.

This technical report has been reviewed and is approved for publication.

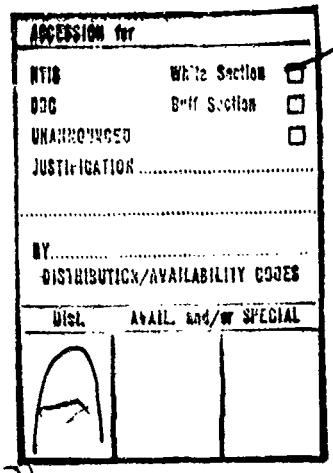

DAVID FISCHER
Project Monitor

WILLIAM G. D. FREDERICK
Chief
Laser & Optical Materials Branch
Electromagnetic Materials Division
Air Force Materials Laboratory

Copies of this report should not be returned unless return is required by security considerations, contractual obligations, or notice on a specific document.

AIR FORCE/56780/31 July 1975 — 100

FOREWORD

This report was prepared by Raytheon Company, Research Division, Waltham, Mass., under Contract No. F33615-73-C-1073, Project 7371, Task 737101, entitled, "Chemical Vapor Deposition of Multispectral Domes." The work was administered under the direction of the Air Force Materials Laboratory, Wright-Patterson Air Force Base, Ohio. Mr. C. T. Ennis, Dr. G. Edward Kuhl, and Mr. D. W. Fischer, AFML/LPO, were project engineers.

At Raytheon, the investigation was carried out in the Advanced Materials Department. Dr. J. Pappis is the Department Manager, and Mr. B. A. diBenedetto was the principal investigator.

This is the Final Technical Report for Contract F33615-73-C-1073. It covers the period 19 March 1973 to 19 September 1974. The report was given the Raytheon internal number S-1792.

The report was submitted by the authors December 1974.

TABLE OF CONTENTS

LIST OF ILLUSTRATIONS

List of Illustrations (Cont'd)

LIST OF TABLES

1.0 INTRODUCTION

Large multispectral windows and domes that are capable of transmitting from the visible to the infrared (~0.5 to 13.5 μm), and also have the requisite physical characteristics to withstand environmental conditions, would greatly simplify system designs and space requirements problems in a number of FLIR and infrared imaging systems. For this reason considerable effort has gone into the development of a single material which will perform adequately in all of the spectral regions of interest. Our approach to this problem has been based on our understanding of the chemical vapor deposition process, the material requirements for infrared windows for reconnassance, and weapon delivery applications, and the experience gained under Contracts No. F33615-70-C-1577, F33615-71-C-1775, F33615-71-C-1779, and F33615-72-C-1501. Under these programs we have successfully fabricated by the chemical vapor deposition process materials such as zinc sulfide, zinc selenide, cadmium sulfide and solid solutions of these materials.

Chemical vapor deposited zinc selenide meets the optical requirements of many FLIR systems, but its hardness and strength appear to be too low to meet environmental conditions. CVD zinc sulfide, on the other hand, is adequate structurally, and the best optical quality material of our most recent deposits has adequate transmission at the wavelengths of interest. Zinc sulfoselenide and zinc-cadmium sulfide solid solutions offered still another choice with unique physical and optical property compromises. Under Contract No. F33615-72-C-1501 all of these materials were produced and evaluated, and the necessary technology was developed that enabled us to improve the transmission, hardness, and strength of each candidate material.

The present program was concerned with the optimization of the physical and optical properties of zinc sulfo-selenide and zinc sulfide, along with the development of techniques for the preparation of domes and plates of the requisite sizes. In addition, the techniques developed will allow these materials to be produced in large quantities at significantly lower costs than heretofore attainable.

2.0 THE CHEMICAL VAPOR DEPOSITION PROCESS

The chemical vapor deposition (CVD) process offers many advantages over conventional techniques for preparing infrared transmitting materials. Perhaps the two most significant advantages are that the resulting material is very pure, and IR absorptions due to impurities are minimized. In addition, the deposits are usually very dense, and thus light scattering due to pores is minimized. Furthermore, the process is not inherently size limited and it has the potential of fabricating polycrystalline infrared windows in large sizes and various shapes.

The chemical vapor deposition process can be summarized as follows: Volatile compounds of the elements comprising the material to be deposited are reacted at a surface whose temperature allows the compound to decompose or react to form a solid, adherent coating. If the coating thickness is heavy enough a monolithic, free-standing plate is obtained. The volatile byproducts of the reaction are pumped away, flushed away in a stream of carrier gas, removed by reaction with a mass of suitable material in the system, or regenerated or used by reaction with a reservoir of a suitable raw material. Figure 1 schematically illustrates the apparatus used in this program.

Chemical vapor deposition processes can be used to form the most refractory substances at temperatures where their vapor pressure is negligible. The properties of the deposited materials can be significantly and controllably altered by the co-deposition of alloying atoms. Depending on the relative concentration of the reactants, either solid solutions or two-phase composites can be formed. Crystallite orientation and size distribution can be controlled by proper manipulation of the deposition parameters. Composites with alternating layers or two or more different materials can be prepared by cycling the composition of the vapors from which the materials are deposited.

Two general types of systems, static and dynamic, can be used for chemical vapor deposition. The static system is a closed system in which the reactants and products are sealed in a chamber. Well-known examples

PBN-366

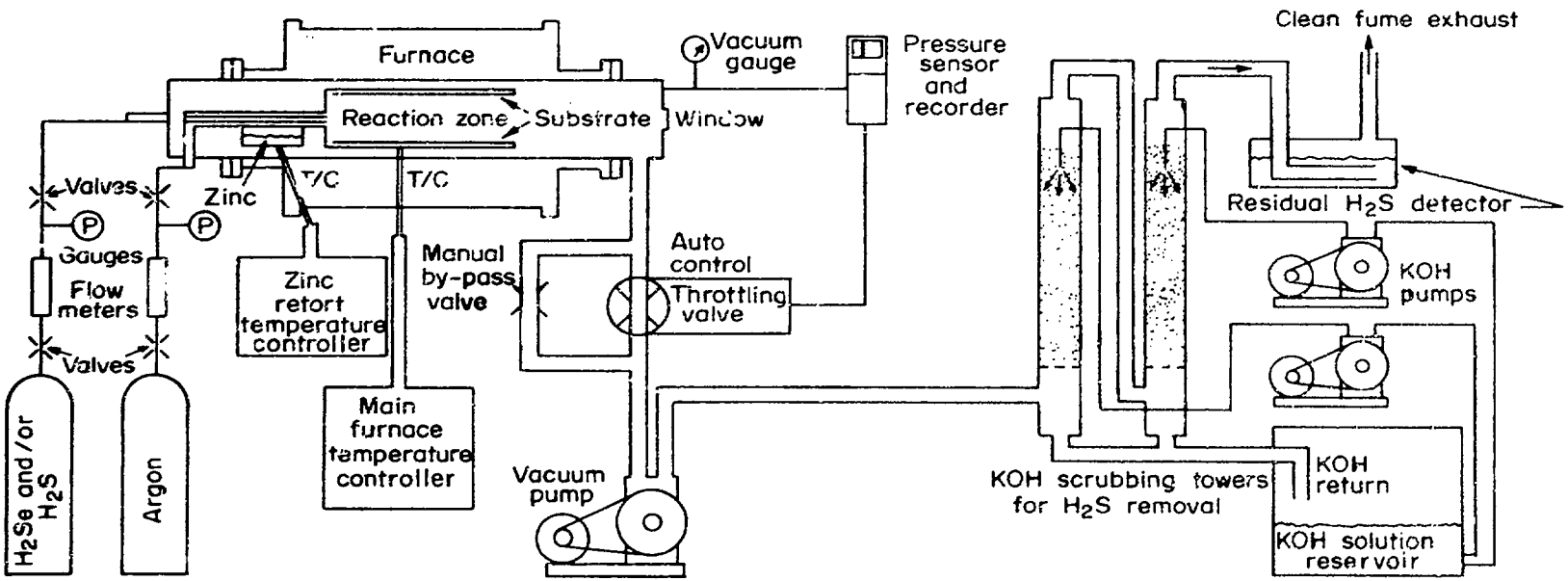

Figure 1. Schematic of ZnS CVD System

are the quartz-iodine incandescent lamp and the hydro-thermal bomb for the deposition of synthetic quartz. In the dynamic system, on the other hand, fresh reactants are continuously metered into the deposition chamber, and the spent vapors are continuously removed, usually by pumping. The reactive gases are fed into the furnace through a gas-metering system. The substrate upon which the deposit occurs is maintained at an appropriate temperature by means of a heater that is inductively or resistively heated. Most vapor depositions are made at pressures on the order of one-hundredth of an atmosphere, although a much higher or lower pressure can be employed.

Our experiments have shown that the dynamic system yields good results in the deposition of zinc and cadmium sulfide and zinc selenide, and solid solutions of these materials, and is preferable because it offers certain advantages. Chief among these is the depletion of reactants and the accumulation of waste materials which are major problems in the static system, are minimal in the dynamic system which allows the addition and removal of materials during deposition. In order to obtain a deposit, the temperature of the substrate chamber and the vapor source are usually more critical and interdependent in the static system than in the dynamic system. The static system, in general, offers less flexibility in the deposition parameters than the dynamic system, since vapor transport is controlled by temperature gradients rather than pressure gradients and mass flow. In addition, the static system is often more susceptible to vapor phase nucleation and particle growth near the substrate; to reduce this effect the partial pressures of the reactive vapors must be low, resulting in low deposition rates. The reactive vapor concentrations are also limited by the equilibrium constants of regenerative reactions and by the fact that partial pressures of the regenerative vapor cannot (for safety reasons) usually greatly exceed one atmosphere. Finally, outgassing of deposition chamber and substrate are of greater importance in the static system than in the dynamic system.

Two general techniques can be employed in vapor deposition. These are: 1) Conventional chemical vapor deposition where the vapor source

temperature is lower than the substrate temperature; 2) Transport chemical vapor deposition where the vapor source temperature is greater than the substrate temperature.

In conventional chemical vapor deposition, the thermodynamics and kinetics of the chemical reactions are such that formation of the solid product is favored at the higher temperatures, whereas the volatile reactants tend to be formed or are stable at the lower temperatures.

In chemical transport deposition, on the other hand, the thermodynamics and kinetics of the chemical reactions are such that formation of the solid product is favored at the lower temperatures, whereas the volatile reactants are formed at the higher temperatures. The deposition of II-VI compounds is best accomplished by use of the dynamic chemical vapor deposition technique. This method was used exclusively for the fabrication of the materials discussed in this report.

3.0 EXPERIMENTAL

3.1 Introduction

Zinc sulfide and zinc sulfo-selenide compositions have been developed in this laboratory under Contract No. F33615-72-C-1501 for multispectral window applications covering a wide spectral range, from the visible to the infrared (~0.5 to 13.5 μm). The successful development of these window materials was accomplished using the chemical vapor deposition process (CVD). Table 1 summarizes some of the more pertinent properties of these materials. The potential of using these materials as windows for a variety of sensors in reconnaissance and weapon delivery systems resulted in the current effort.

To further develop these materials required additional improvement in their optical quality and the scale-up of the process to fabricate large size plates and hemispherical domes with the required properties. In the case of zinc sulfo-selenide solid solutions, control of index of refraction variation remained a problem. In the case of both the sulfo-selenide and the pure sulfide, optical scatter in the near infrared and the visible caused reduced transmission in that region. Additional insight as to the identity and source of these scatter sites was of primary concern. A final concern was to enhance the resistance of the materials to airborne environmental conditions, while not degrading their optical quality.

The program progressed in six interrelated areas of development; zinc sulfo-selenide, large plates of zinc sulfide, zinc sulfide domes, microstructural analysis, scatter analysis, and zinc sulfide surface coating of zinc selenide. A number of process and scale-up deposition trials were carried out in the CVD deposition system schematically represented in Figure 1. Modifications and additional controls were added to this apparatus as needed for specific run requirements. Physical and optical property evaluations were carried out on each deposition with special attention being given to microstructure, scatter, and hardness analysis. In following sections a

TABLE 1

TYPICAL CVD MATERIALS PROPERTIES

Property	Standard ZnSe	ZSS	ZnS
Density (gm/ cc)	5.27	5.15	4.08
Refractive Index (8-13 μm)	2.40	2.38	2.20
Transmission (8-13 μm)	> 69%	(see transmission spectra)	
Transmission Limits (μm)	0.5 - 22	(see transmission spectra)	
Hardness (Knoop 50 gm, kg/ mm^2)	100	190	215
Absorption Coefficient at 10.6 μm (cm^{-1})	0.002-0.005	0.007	0.22
Grain Size (microns)	70	100	20-100
Flexural Strength (psi, 4-point loading)	6500	----	15,000
Young's Modulus (psi, $\times 10^6$)	9.75	0.16	10.8
Thermal Expansion (RT-500° C, $\times 10^{-6}$/° C)	8.53	8.30	7.85
Thermal Conductivity (RT) (cgs) 25° C	0.043	0.02	0.040
Specific Heat (cal/ gm/ ° C)	0.085	0.083	0.112
Electrical Resistivity (ohm-cm)	$\sim 10^{12}$	$\sim 10^{12}$	$\sim 10^{12}$

description of the progress made in each of the areas mentioned above, along with a description of a 10 × 10 × 5/8 in. plate and 9-inch diameter dome produced at the conclusion of the program.

3.2 Zinc Sulfo-Selenide Solid Solutions

Zinc sulfide and zinc selenide form a continuous solid solution. In these mixed crystals the multiphonon and visible range transmission cutoffs contain characteristics of both the pure ZnS and ZnSe, the overall effect of which is to shift the cutoffs to longer wavelengths as the percentage of selenium is increased. CVD deposits with compositions throughout the composition range were prepared and reported under Contract No. F33615-72-C-1501. It was established that 10% zinc sulfide-90% zinc selenide composition provided transmission over the desired spectral range and in addition exhibited increased strength and hardness due to solid solution hardening phenomena.

In our previous work the solid solutions were deposited by reacting zinc vapor with hydrogen sulfide and selenide gases according to the reaction:

$$Zn(v) + xH_2S(g) + (1-x)\,H_2Se(g) \rightarrow ZnS_xSe_{(1-x)}(s) + 2H_2(g)$$

It is known that the dissociation thermodynamics and kinetics of H_2S and H_2Se are dissimilar and that one could not expect the reaction rate of zinc and selenium (or a selenium compound) to be the same as the reaction rate of zinc and sulfur (or a sulfur compound) at a given temperature. Therefore, fabrication of plates and domes of the desired sizes with constant composition and homogeneous properties throughout, requires that the varying reaction rates be established and that the proper concentrations of reaction species be available at the growth interface at all times. It follows thus that tight control is required of all the pertinent process parameters.

The refractive index of zinc sulfide is 10 percent lower than that

of the selenide (2.20 vs 2.40) in the 8 to 13 μm range used in long wavelength passive infrared systems. The refractive index of a specific solid solution can be estimated by simple linear interpolation between these two limits. Thus a 10 percent sulfide substitution would result in a refractive index near 2.38. A 1 percent variation in an absolute sulfide concentration will produce a change of 2×10^{-3} in refractive index. Thus an rms transverse composition change of 5×10^{-4} or less is required to keep the rms refractive index to the desired level of 10^{-4}. This is a very tight restriction, and is unlikely to be met at all times during deposition. Fortunately, the restriction in refractive index change can be relaxed substantially if that variation occurs in a direction normal to the plane of an optical surface, that is, along the appropriate ray direction. Fortunately this is the situation in stratified CVD materials. Furthermore, if the lateral variations, when they do occur, are in high spatial frequencies, that is, over a very small spatial scale, the resultant scattering will simply add to the diffuse background rather than to degradation of the small-angle image sharpness. The deposition of solid solution compositions which permits visible image resolution therefore requires that the regions of index variation be very small, or that the bands (i.e., layers of slightly different composition) be normal to the direction of image propagation.

During the course of this program thirty-seven (37) zinc sulfoselenide depositions were carried out. The primary objective of these process runs was to improve control over all process parameters in order to reduce banding and image distortion due to the index variations described above. Process parameters such as temperature, pressure, zinc vaporization rate, H_2S-H_2Se gas mixing, foreign ion doping, mandrel material and shape, gas flow patterns, etc. were all examined closely. Details of process conditions used for these runs are reported in Table 2.

The composition of the solid solution deposit from each run was established by taking representative samples from the mixing chamber, top, middle, bottom, and exhaust chamber of each run and determining their lattice parameters. A General Electric XRD-5 X-ray diffractometer using CuKα

TABLE 2

DEPOSITION CONDITIONS

Run No.	Mandrel Temp (° C)	Furnace Press. (torr)	Zn Retort Temp (° C)	H_2S Flow (lpm)	H_2Se Flow (lpm)	Deposition Time (hrs)	Zn Pick-up Rate (gm/hr)
ZSS-26	750	60	590-620	0.5	0.5	20/40	100 avg.
ZSS-27	750	60	590-610	0.5	0.5	20/10	85 avg.
ZSS-28	750	60	590	0.5	0.5	60	60
ZSS-29	750	60	590	0.5	0.5	60	60
ZSS-30	650	60	550	0.5	0.5	10	low
ZSS-31	825	60	655	0.5	0.5	24	95
ZSS-32	750	60	590	0.5	0.5	17	60
ZSS-33	825	60	625	0.5	0.5	24	37
ZSS-34	650	60	690	0.5	0.5	24	60
ZSS-35	650	60	620	0.5	0.5	24	95
ZSS-36	630	60	690	0.5	0.5	24	70
ZSS-37	650	60	590	0.5	0.5	24	40
ZSS-38	650	60	600	0.5	0.5	36	62
ZSS-39	650	60	595	0.5	0.5	30	60
ZSS-40*	650	60	590	0.5	0.5	20	60
ZSS-41**	650	60	590	0.5	0.5	24	60
ZSS-42	650	60	590	0.5	0.5	24	60

*plus 0.035 lpm O_2

**plus 0.07 lpm O_2

Table 2 (Cont'd)

Run No.	Mandrel Temp (° C)	Furnace Press. (torr)	Zn Retort Temp (° C)	H_2S Flow (lpm)	H_2Se Flow (lpm)	Deposition Time (hrs)	Zn Pick-up Rate (gm/hr)
ZSS-43	650	60	595	0.5	0.5	24	60
ZSS-44	650	60	600	1.0	0.5	24	60
ZSS-45	650	70/55/40	600	0.5	0.5	10/10/10	60 avg.
ZSS-46	650	60	600	0.5	0.5	8	low
ZSS-47	650	60	600	0.5	0.5	30	60
ZSS-48	650	60	600	0.5	0.5	48	60
ZSS-49	670	60	600	0.5	0.5	54	60
ZSS-50	750	60	600	0.5	0.5	30	90
ZSS-51	700	60	595	0.5	0.5/0.0	12/5	80
ZSS-52	700	60	600	0.5	0.5	30	90
ZSS-53	660	60	600	0.5	0.5	20	60
ZSS-54*	660	60	600	0.5	0.5	32	80

*plus 0.035 lpm O_2

radiation was employed for an initial scan. Then representative high-angle diffraction peaks (usually the (620), (533), and (711) peaks) were step-scanned at 200 sec per step using 2θ increments of 0.05° to obtain an accurate "d" spacing for lattice parameter calculations. This parameter was then compared to a plot of the published values of solid solution composition as a function of lattice constant in order to identify the composition of the unknown sample. The lattice constants and composition of each run are summarized in Table 3.

The Knoop hardness using a 50-gram load was measured on samples taken from an area on the mandrel immediately adjacent to each of the lattice constant samples. The results of these hardness tests are given in Table 4. The hardness of most of these deposits was in the range Kn = 200 to 250 as was expected from the previous work on these compositions.

The in-line transmittance from 2.5 to 40 μm was measured on polished samples taken from the top, middle, and bottom of each deposit. A Perkin-Elmer 457 Grating Infrared Spectrometer was used for this purpose. The aperture size was approximately 0.2 $in.^2$ and sample thickness varied from 0.100 to 0.400 in. depending on the thickness of the deposit. A representative transmittance curve for a good visible imaging quality* deposit with approximately 7 percent zinc sulfide is shown in Figure 2.

One of the first concerns in the deposition of improved homogeneity solid solutions was to install a more precise temperature control system. It was felt that the zinc pickup rate, the difference in deposition rates of zinc sulfide and zinc selenide, as well as the microstructure would vary beyond tolerable limits without precise temperature control. New temperature control systems for both the retort heater and main heater were designed and installed for run ZSS-35 (see Figure 1). On subsequent runs, adjustments

*Visible imaging quality as used here and throughout this report refers to the relative ability of the naked eye to clearly discern images such as typewritten letters through a given thickness of the material at distances of at least two to three feet.

TABLE 3

LATTICE PARAMETER AND COMPOSITIONS OF ZINC SULFO-SELENIDE DEPOSITS

Run No.	Mixing Chamber		Mandrel Bottom		Mandrel Middle		Mandrel Top		Exhaust Chamber	
	Lattice Param.	Compos. % ZnS	Lattice Param.	Compos. % ZnS	Lattice Param.	Compos. % ZnS	Lattice Param.	Compos. % ZnS	Lattice Param.	Compos. % ZnS
ZSS-26									5.640	11.0
ZSS-27							5.655	5.0	5.653	6.0
ZSS-28			5.646	8.0			5.650	7.0	5.646	8.0
ZSS-29									5.648	7.5
ZSS-30							5.664	2.5		
ZSS-31							5.641	10.0	5.624	17.0
ZSS-32	5.650	7.0	5.652	6.0	5.652	6.0	5.651	6.5		
ZSS-33			5.651	6.5	5.651	6.5	5.650	7.0		
ZSS-34			5.655	5.0	5.657	4.5	5.656	4.7		
ZSS-35					5.647	8.0				
ZSS-36			5.653	5.5	-----	---	5.654	5.5		
ZSS-37			5.657	4.5	-----	---	5.657	4.5		
ZSS-38			5.650	7.0	5.652	6.0	5.652	6.0		
ZSS-39							5.642	10.0		
ZSS-40							5.653	5.5		
ZSS-41					5.651	6.5				
ZSS-42					5.642	10.0				

Table 3 (Cont'd)

Run No.	Mixing Chamber		Mandrel Bottom		Mandrel Middle		Mandrel Top		Exhaust Chamber	
	Lattice Param.	Compos. % ZnS	Lattice Param.	Compos. % ZnS	Lattice Param.	Compos. % ZnS	Lattice Param.	Compos. % ZnS	Lattice Param.	Compos. % ZnS
ZSS-43			5.651	6.5	5.655	5.0	5.655	5.0		
ZSS-44					5.647	8.0	5.645	8.5		
ZSS-45			5.651	6.5	5.653	5.5	5.654	5.5		
ZSS-46					5.654	5.5	5.654	5.5		
ZSS-47					5.656	4.7	5.654	5.5		
ZSS-48					5.655	5.0				
ZSS-49			5.651	6.5	5.653	5.5	5.652	6.0		
ZSS-50			5.617	20.0	5.634	13.0	5.638	11.5		
ZSS-51					5.411	100.0				
					5.653	5.5				
ZSS-52			5.627	16.0	5.633	13.5	5.633	13.5		
ZSS-53			5.655	5.0	5.655	5.0				
ZSS-54			5.647	8.0	5.647	8.0	5.654	5.5	5.655	5.0

TABLE 4

KNOOP HARDNESS (50 gm load) OF ZINC SULFO-SELENIDE DEPOSITS

Run No.	Mixing Chamber	Mandrel Bottom	Mandrel Middle	Mandrel Top	Exhaust Chamber
ZSS-26	---	184	180	186	186
ZSS-27	---	169	177	184	---
ZSS-28	---	202	---	196	188
ZSS-29	---	---	---	---	192
ZSS-30	---	---	---	---	---
ZSS-31	---	---	---	168	184
ZSS-32	212	173	192	182	---
ZSS-33	---	153	156	---	---
ZSS-34 (sub)	---	224	218	226	---
ZSS-34 (dep)	---	170	179	169	---
ZSS-35	---	---	208	---	---
ZSS-36	---	231	---	---	---
ZSS-37	---	230	---	229	---
ZSS-38	---	220	223	219	---
ZSS-39	---	235	230	235	---
ZSS-40	---	217	215	227	---
ZSS-41	---	---	221	---	---
ZSS-42	---	227	209	205	---
ZSS-43	---	202	212	216	---
ZSS-44	---	---	221	230	---
ZSS-45	---	228	217	181	---
ZSS-46	---	256	249	217	---
ZSS-47	---	178	196	189	---
ZSS-48	---	223	210	207	---
ZSS-49	---	235	247	220	---
ZSS-50	---	212	192	185	---

Table 4 (Cont'd)

Run No.	Mixing Chamber	Mandrel Bottom	Mandrel Middle	Mandrel Top	Exhaust Chamber
ZSS-51	---	222	226	198	---
ZSS-52	---	204	215	226	217
ZSS-53	---	249	238	232	---
ZSS-54	---	235	233	224	---
ZSS-55	---	244	230	220	---
ZSS-56	---	---	---	154	---
ZSS-57 (sub)	---	233	189	174	---
ZSS-57 (dep)	---	176	158	197	---
ZSS-58	---	206	196	202	---
ZSS-59	260	251	260	245	---
ZSS-60	---	---	---	---	-

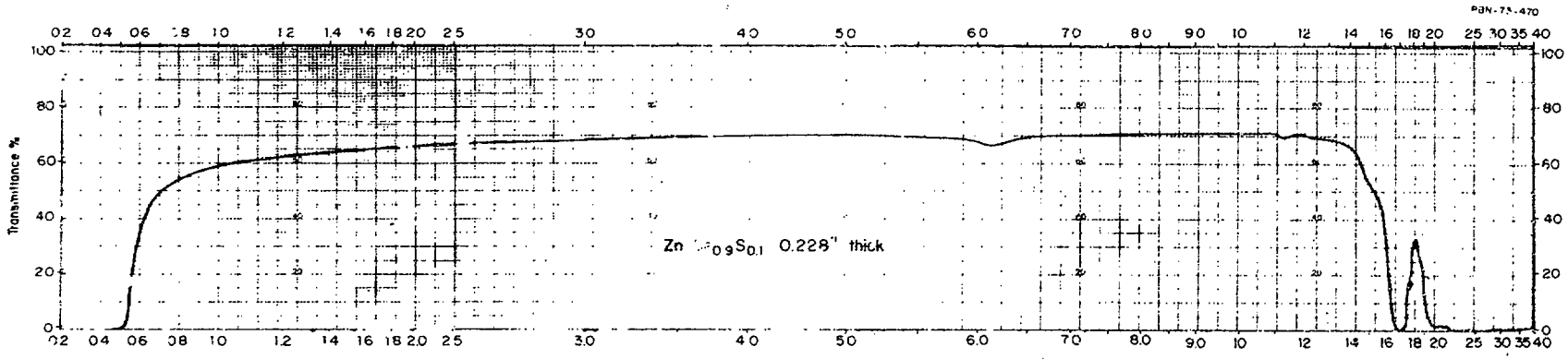

Figure 2. Typical In-Line Transmission Curve (0.5 to 22 μm) for CVD Zinc-Sulfo-Selenide Solid Solution

were made in order to optimize the effective temperature control. In one of these runs, ZSS-37, for a period of time the temperature controller was set so that there was a sinusoidal temperature fluctuation of $\pm$ 3° C. Discrete bands were evident in the resultant deposit which were directly correlated to each temperature oscillation. These slight index changes reflect slight changes in the solid solution composition due to one or more of the previously mentioned temperature dependent phenomena variation. In all subsequent runs, therefore, both temperature controllers were employed and functioned well. In ZSS-47 and ZSS-48 temperature was closely controlled and monitored for deposition periods of 30 and 48 hours respectively. The measured temperature deviation was less than 1° C. Though other conditions in the process such as turbulence still caused compositional variations during these runs, the effect of improved temperature control was clearly evident. In run ZSS-47, for example, splitting of the α_1 and α_2 x-ray peaks was more pronounced than normal, indicating improved homogeneity over any previous runs with a similar composition. Precise temperature control was therefore shown to contribute substantially to improved quality of solid solution deposits and conversely, slight temperature interruptions were shown to cause discrete banding.

Pressure control was a second process parameter which was believed to have an influence on the resultant optical quality of the zinc sulfo-selenide deposits. First of all we investigated the effect of furnace pressure on the optical quality of the deposited material. Run ZSS-45 was a 30-hour deposition with the deposition period divided into three 10-hour deposits where the pressure was dropped in steps, from 70 torr to 55 torr to 40 torr. The optical quality of each region showed a definite variance sharply marked at the time of pressure change. It is believed that the primary difference is a compositional change that is caused by, 1) progressively decreasing residence time, and 2) the difference in zinc usage rate with pressure. This run pointed up the special need for good furnace pressure controls when working with solid solution compositions.

In order to improve the pressure control several electronic and pneumatic automatic pressure control systems were investigated early in the program. A pneumatic system which was compatible with the existing furnace and vacuum pumping equipment was chosen and installed. In this

system a diaphram sensor in the controller senses the vacuum and feeds deviations from the control point back to a completely automatic pneumatic valve in the vacuum pump foreline (Figure 1). Also included in this system is an 8-day recorder which continuously records the furnace pressure. Check-out evaluation using mock-up process conditions showed precise control over 12 hours to less than 0.1 torr (reading sensitivity of the meter). The system was first tested under full run conditions in run ZSS-59, and was used on all subsequent runs. Correlation of the pressure dependence on improvements in the optical quality of these deposits was realized mainly in regard to the pressure dependence of zinc usage rate, rather than the actual pressure fluctuations themselves.

It was known that one of the causes of layers and banding in the solid solutions was the variable usage rate of zinc as a function of time. Zinc usage rate, i.e., zinc evaporation rate, becomes the zinc vapor flow rate into the mandrel area. Obviously the amount of zinc vapor available for reaction with H_2S and/or H_2Se for each increment of time will have an influence over the quality and composition of the deposit for that increment of time. The degree to which this effect was detrimental was established in several runs such as ZSS-26 where the run was made under conditions which would produce the good optical quality material for the first 20 hours of deposition. For the next forty hours of the deposit the zinc usage rate was doubled. Evaluation of this material showed that the visible imaging quality of the first deposited material was significantly better than that deposited over the last forty hours.

Innovative attempts to control and monitor the zinc pickup rate were evaluated throughout the course of the program. Temperature and pressure control as previously mentioned were of course necessary since the vaporization rate can only be as constant as the temperature and pressure of the evaporation chamber. The vaporization rate is also dependent on the evaporation surface area. To insure that the surface area remained constant in run ZSS-27 a retort was designed to virtually eliminate the oxide (slag layer) from the melt surface. By eliminating the slag layer from the zinc melt it was felt

that the available zinc evaporation surface would be constant and thus the evaporation rate would be constant. In another run, ZSS-39, a stirring action, via bubbling of argon throughout the zinc melt, was used for the same purpose. Neither of these approaches was developed to the point where they offered any real improvement over the normal zinc surface. It was finally decided that a constant zinc evaporation rate could be realized with tight control of temperature and pressure and the standard retort system. This was graphically demonstrated by monitoring the zinc melt reservoir depletion rate with a linear vertical displacement transducer which continuously monitored the liquid zinc level. A system was designed that indicated deviations as low as 5 grams/hour. This zinc monitoring system was used in all subsequent runs. The zinc evaporation rate deviations in most of these later runs were below the detectable limits of this system.

In order to further reduce potential compositional variations in the solid solutions an external gas premix chamber was also investigated. The H_2S and H_2Se gases were introduced to this chamber from individually metered sources and allowed to premix prior to being introduced to the furnace and reaction zone. Run ZSS-43 was the first run to use this system with all other process conditions being normal. The optical quality of this material was fairly good but no dramatic decrease in banding (i.e., compositional fluctuations) was evident. This indicated that the compositional banding we experienced was not a consequence of poor physical mixing of the input gases.

In our previous work we had found that a 750° C deposition temperature produced the best optical quality solid solution. Under the current work we established that zinc vaporization rate, temperature control, etc. also had an influence on visible imaging quality. It follows thus that we might be able to find conditions for depositing good imaging quality solid solutions at higher or lower deposition temperature by systematically varying other process parameters at other deposition temperatures (i.e., 650° C, 700° C, and 825° C). This would then allow us to take advantage of properties such as smaller grain size, and improved homogeneity for deposits grown at these temperatures.

One of the obvious causes of index of refraction changes in solid solution deposits is composition inhomogeneity or poorly formed solid solutions. One way to improve the formation of solid solutions is to increase the deposition temperature. Thus we expected improved homogeneity for runs deposited at 825° C. Two 24-hour runs, ZSS-31 and ZSS-33, were carried out at a deposition temperature of 825° C. These runs used a high and low zinc usage rate respectively with all other process conditions being common to both. In both cases the visible imaging quality of the material was degraded, with respect to the 750° C deposits, although the visible imaging quality of ZSS-33 (low Zn usage rate) was significantly better than ZSS-31 (high Zn usage rate). As normal with low zinc usage rates, the composition of ZSS-33 was higher in selenium content and this may be the reason for the better visible imaging quality as compared to ZSS-31. The noteworthy point about these two high temperature runs was that the compositional homogeneity, as determined from the sharpness of the x-ray diffraction peaks, was greatly improved over 750° C deposits. In spite of this fact, however, the index variation was greater than that observed in 750° C deposits. This is due to the fact that at a deposition temperature of 825° C the size of the areas of varying index are larger than at a deposition temperature of 725° C.

Material was also deposited at 700° and 750° C to examine the improvement in the index variations with the improved temperature control system. Run ZSS-50 was made at 750° C for 30 hours with less than a $\pm$0.5° C temperature variation. Similarly, ZSS-52 was run at 700° C for 30 hours with comparable temperature control. Analysis of these runs indicated that the visible imaging quality degraded with increasing deposition temperature, but in both cases the visible imaging quality was significantly better than any previous runs deposited at the same temperature. These runs probably represent the practical limit to which we can improve the homogeneity by temperature control alone. The good visible imaging quality in low temperature deposits and lack of powder inclusions in high temperature deposits suggested 700° C (ZSS-52) to be a rather attractive compromise, with the only major distortion occurring from occasional (2 to 3/ cm^2) exaggerated nodular growth areas approximately 1 mm in diameter.

Run ZSS-34 initiated the start of a series of runs at a deposition temperature of 650° C. The purpose of these runs, as noted above, was to determine the effect of deposition temperature on index of refraction variations. The visible imaging quality of this run was considered to be excellent even though there was a dark band in part of the material, and many minute bands throughout the deposit. One possible mechanism for the generation of the powder inclusions is the condensation of fine zinc droplets after the Zn vapor enters the reaction zone and the incorporation of these particles into the material. We reasoned that this was a more serious problem in low temperature deposits where the retort and mandrel temperatures are only 50° C different in temperature. In ZSS-49 we increased the mandrel temperature to 670° C in order to reduce the tendency of Zn to condense in the reaction zone. Otherwise run conditions were the same as the best previous conditions. The deposition was carried out for 54 hours and a reasonably thick (up to 3/16 in. thick) deposit of good optical imaging quality material resulted. Powder inclusion did occur, however, in a band in the middle of the deposit. Since the deposition temperature was held constant during the entire run it is not temperature alone which causes powder inclusions.

A most striking feature of these runs is the difference in microstructure. Figure 3a, b, c illustrate the type of microstructures observed at 650° C, 700° C and 825° C.

It appeared from the previous results that the optimum deposition temperature for zinc sulfo-selenide solid solutions was 650° C provided all other parameters are controlled. One of the consequences of lowering the deposition temperature from 750° C to 650° C was that the deposits contained less sulfur (from ~7% to ~4%) and were therefore softer. In run ZSS-44 the H_2S flow rate was doubled in order to increase the sulfur concentration to ~7%, while still maintaining the low 650° C deposition temperature. The resulting composition for this run was ~8% (see Table 3) as was expected. Even though the optical quality of ZSS-44 was not equivalent to 4% doped material, visible imaging was possible at the higher sulfur content.

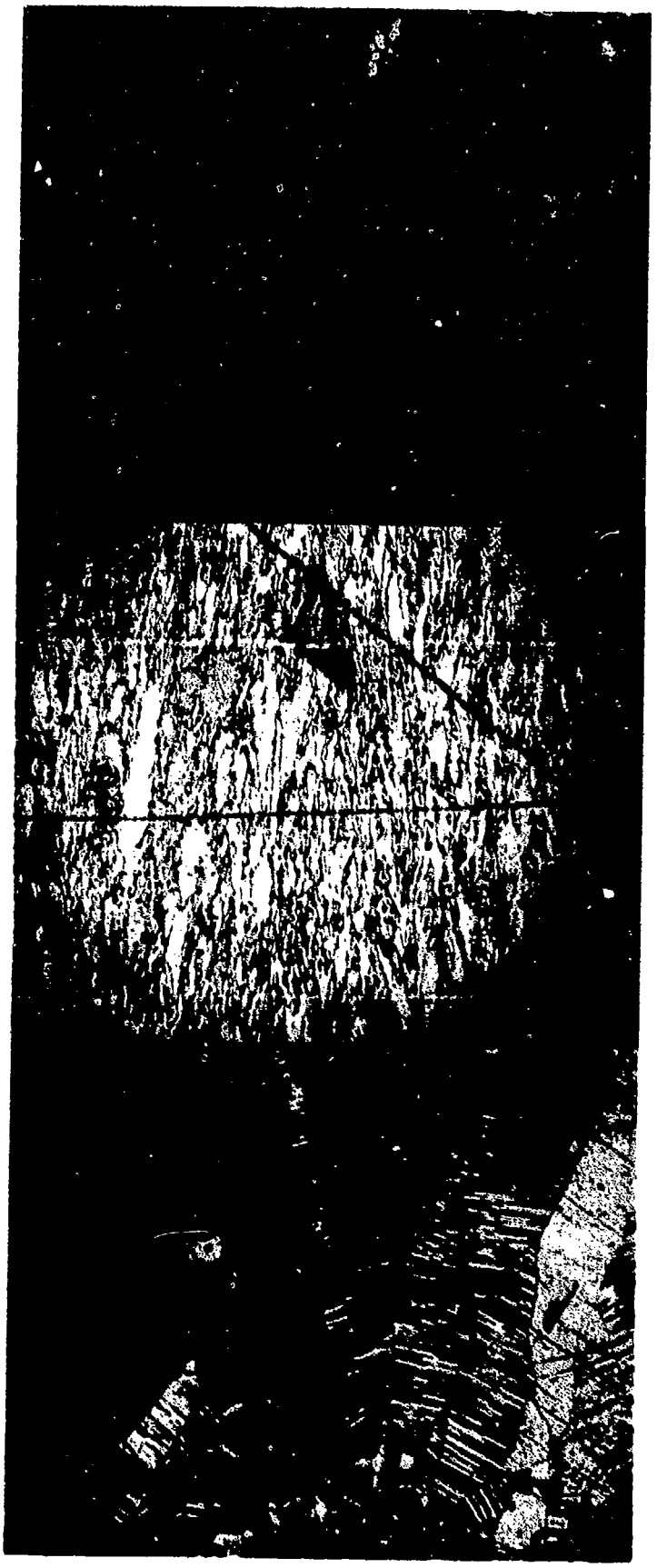

(a)

(b)

(c)

Figure 3. Microstructure of (a) 650° C (b) 750° C and (c) 825° C Deposited Solid Solutions (140X)

There were indications from our previous work that the addition of oxygen to the zinc sulfo-selenide system had the effect of increasing the hardness and also reducing the characteristic 6 μm absorption band found in the lower temperature deposits. The introduction of oxygen should also have an effect on the stacking faults in zinc sulfide and plays a major role in the thermodynamics of the system. During the course of this program thermochemical equilibrium calculations were made for the CVD ZnSe system using a computer program.[1,2] Specifically, the effect of oxygen addition upon the overall gas composition and the resulting effect upon ZnS deposition were explored.

Under typical conditions (650° C and 40 mm pressure), and in the absence of oxygen, the hydrogen sulfide is only 13% decomposed into H_2 and S_2. This contrasts with the CVD ZnSe system in which the hydrogen selenide is more than 90% decomposed under comparable conditions. However, the equilibrium calculations also reveal that small additions of oxygen promote the formation of H_2O which decreases the H_2S concentration while markedly increasing the S_2 concentration in the furnace atmosphere.

ZSS-32 was carried out with oxygen doping during deposition. All process conditions used were identical to our standard 750° C deposition conditions with the exception that 0.035 lpm of oxygen was added to the H_2S/H_2Se flows. Deposition was carried out for 17 hrs. The resultant material had excellent visible imaging characteristics though caution should be exercised in placing too much emphasis on results from thin (0.050 to 0.070 in.) samples. As a minimum, however, the use of oxygen reduced the 6 μm absorption band in this sample.

The purpose of runs ZSS-40 and -41 was to examine the effect of oxygen gas on the visible imaging quality of the already improved imaging quality 650° C material. In ZSS-40, 0.035 lpm O_2 was added to the input gases and in ZSS-41 this was doubled to 0.07 lpm. Both of these runs contained areas where the visible imaging quality was excellent. There were, however, areas of powder inclusion in the center of each plate which decreases the total

transmission at shorter wavelengths. The reduction of the 6 μm absorption when oxygen gas was used in 750° C material was not as pronounced in the 650° C deposits. ZSS-41 also showed considerable cracking and sticking to the mandrel. This was probably due to corrosion of the mandrel by the higher oxygen gas flow.

In viewing samples parallel and perpendicular to the deposition plane it is apparent that the best visible imaging quality material is obtained when the layers of differing index of refraction are flat and parallel. This indicates that good visible imaging quality material can be obtained even if the bands are not completely eliminated. What is required is that the deposit conform in geometry as closely as possible to the geometric form of the intended optical component; secondly, deposits should be made so as to minimize the lateral scale of any perturbation in the growth pattern (i. e., nodular growth).

With this thought in mind, run ZSS-28 was made using specially polished graphite mandrels. This run resulted in material at least equivalent to the best deposited. Except for a few localized areas, the bands were all relatively flat and parallel. In run ZSS-29 several mandrel surfaces, polished graphite, deliberately roughened graphite, polished molybdenum, and polished fused silica, were evaluated to determine the effect that the initial deposition surface has throughout the entire growth process (for example, a 60 hr deposit). All other process conditions in this run were identical to ZSS-23.[1] The results of this run indicated that there was no measurable difference in visual imaging quality of material grown on the various mandrel materials. On examining cross-sections of deposits from each mandrel material it was noted that if the mandrel is smooth the deposition interface starts out flat (as noted from flat bands). However, in all cases there were several discrete times during the deposition that a nodular growth was initiated. This growth is apparently due to a sudden inclusion of sizable vapor phase particles (as noted from the sudden waviness of the band structure). Nevertheless, this evaluation shows that it is necessary to have a flat, well polished mandrel to give a good start to the deposit. To eliminate the introduction of nodular growth during deposition is a different, more critical problem.

One additional mandrel evaluation that is worthy of note was that in ZSS-34 a polished plate of ZnSe was used for the mandrel on one side of the reaction zone. The deposit, though it showed no unusual optical quality, did separate from the zinc selenide mandrel, indicating that zinc selenide can be used as a mandrel material in special cases where a reentrant shape with replicated polished surfaces are required.

One other cause of scattering and index of refraction variation in these materials is believed to be the inclusion of vapor phase reacted material in the matrix of the deposit material. This material is to be contrasted to material that is reacted at or near the mandrel wall. Vapor phase reacted material may or may not be of the same composition as the matrix material and it may or may not be of the same crystal structure as material reacted near the wall. Vapor phase reacted material can be enhanced by turbulence within a mandrel and by high input concentrations of the reactants.

In an attempt to minimize turbulence in the gas flow a conical mandrel configuration was designed that eliminated protrusions. Two runs, ZSS-36 and -37, used this design. The resultant deposits yielded reasonably good visible imaging quality material. There was no evidence of powder formation which could be ascribed to a vapor phase reaction as a consequence of turbulence. There was, however, no reduction in the index variations which manifest themselves as bands when the samples are examined in cross-section. It appears that redesign of the mandrel did not have the dramatic effect we would have desired and that reduction of turbulence by considering new nozzle designs might be a more fruitful approach.

Our nozzle design in all runs up to ZSS-46 was a straight hole 0.1 in. in diameter. In ZSS-46, -47, and -48 we used a 0.2 in. diameter straight hole. This was to reduce the velocity of the gases and provide a less turbulent spreading plume. ZSS-47 and -48 were long runs and definitely showed the gas nozzle design to be an area of concern. The lower velocity gas input did apparently provide a less turbulent flow in the early stages of the run. However, growth occurred around the nozzle area and in effect continuously

varied the nozzle position and design. As a result the composition of the material can vary continuously since the kinetics of the reaction are being continuously altered. Before further improvements to the nozzle design could be realized we had to concern ourselves with reducing growth in the nozzle area and the interference that this growth produces.

In order to discourage growth around the nozzle we redesigned our input gas system so that the H_2S-H_2Se gas mixture was surrounded by a concentric argon gas byflow. This meant that in order for growth to occur in the vicinity of the nozzle, zinc would have to diffuse through the argon flow stream. This injector system was first tried on ZSS-53, but was unsuccessful because the nozzle area was too cool and large drops of zinc consensed. However, the same system with a 2 in. graphite extension, which circumvented the condensing problem, was used in ZSS-54 with complete success. The nozzle area, for the first time in any of our solid solution deposits was completely free of growth at the completion of the run. Thus the flow pattern which the nozzle defines at the beginning of a run was maintained throughout the run. With this solution to the problem of growth around the nozzle one can proceed to look at more details of the input gas flow patterns.

Another method of reducing vapor phase reactions and perhaps banding is to increase the mandrel cross-sectional area and reduce variations in the gas composition in the mandrel volume. In run ZSS-39 a 6 × 6 in. cross-section mandrel was used. This mandrel is nearly three times the cross-sectional area of the standard mandrel. All other process conditions used for this run were similar to previous runs. The results of this deposition indicated that visible imaging quality of the material was good. It was free of any obvious powder inclusions; however the bands of varying index were still present to approximately the same degree as previous runs. One significant result of the increased mandrel cross-section is that for same input ratios of H_2Se and H_2S the percentage of ZnS in the deposit is significantly higher in comparison to other standard deposits (Table 4).

The final objective of the zinc sulfo-selenide development program was to establish procedures for the fabrication of plate and dome shapes of requisite thickness. Run ZSS-38, a 36 hour deposit, was the start of a series of longer deposition runs. Its purpose was to examine the effect of longer deposition time on homogeneity in the thicker depositions which eventually will be required. This deposition was approximately 3/16 in. thick with a reasonably good thickness profile. Although the visible imaging quality of this first run was limited by the formation of bands, subsequent runs of equal duration showed that as long as control can be maintained over the process parameters previously discussed homogeneity can be maintained.

One of the primary concerns when considering the growth of large, thick plates is the deposition rate. In ZSS-55 we initiated a series of runs to examine what process adjustments would have to be made to increase the deposition rate. The flow rates of H_2S and H_2Se were increased by 50 percent in this run for that purpose. In order to maintain the same H_2S and H_2Se to Zn input molar ratio it was necessary to correspondingly increase the Zn pickup rate. This was accomplished by increasing the Zn retort temperature. In this run the mandrel temperature was also raised to maintain the desired temperature difference between the mandrel and retort. The deposit from this run had areas of good optical imaging quality, and the growth rate was increased 30 to 40 percent.

Run ZSS-58 was a further attempt to increase the growth rate by increasing the H_2S and H_2Se flows 100 percent over normal conditions. Again, the Zn pickup rate had to be adjusted to maintain the desired molar ratio. This resulted in the desired zinc pickup rate that in turn increased the growth rate to the desired value (~ 8.5 mils/hr). The optical quality of the deposit, however, was not as good as that obtained for the lower deposition rate deposits. It is possible that we may have to limit the rate at which the material is deposited to obtain the desired optical quality material.

In run ZSS-59 a fifteen-inch long mandrel was used to determine what the compositional gradient would be for plates of this size. The operating

conditions used were similar to those used to deposit what was considered to be the optimum composition which includes the use of 0.035 lpm of O_2 gas with the H_2S and H_2Se gases. Prior to depositing the solid solution a thin layer of zinc sulfide was deposited and the sulfo-selenide graded into this layer. The material deposited from this run was of good optical quality. The deposition rate was 2 to 3 mils per hour. The thickness profile did not vary more than 20 percent over the entire length of the plate. The composition of the material is considered to be quite good over the entire length of the plate and the area from which a 10 X 10 in. sample could be cut would not vary more than 1 percent.

Run ZSS-60 was carried out in a furnace with a large seventeen (17) inch element that would be required for the large plate deposits. This run was made at a deposition temperature of 700° C. The temperature profile of this furnace was sufficiently different from other furnaces such that it was not possible to obtain the desired zinc flow rate for a prolonged period of time. Thus the run was terminated after 24 hours. The material from this run, although thin, was of good optical quality.

A dome mandrel was inserted at the top of run ZSS-29 in order to determine the type of problems that would arise in the fabrication of domes. A reasonable, sound dome with a good thickness profile was obtained. The overall visible imaging quality of this run was reasonable considering it was deposited during the first stages of the program. Further dome development work was directed towards pure zinc sulfide. This work is discussed later in the report.

Although the major emphasis of this program was redirected to pure zinc sulfide development at this time it is felt that the work on CVD zinc sulfo-selenide solid solutions resulted in the development of a useful material for specific applications. High optical quality zinc sulfo-selenide deposits can be prepared with properties similar to those listed in Table I. Perhaps the most significant value of this work, however, was the development

of control systems for all process parameters of importance. Furthermore, the technology that was developed was applicable to the zinc sulfide deposition work and helped immeasurably in depositing optimum optical quality material.

3.3 Large Zinc Sulfide Plates

A second task of this program was to develop techniques for the preparation of large zinc sulfide plates (10 × 10 × 5/8 in.) for FLIR systems which operate in the visible, at 1.06 μm, as well as the 8 to 10 μm range. Approximately half way through the program the emphasis was shifted from sulfo-selenide to pure sulfide plate development.

Stoichiometric, pore-free and structurally homogeneous zinc sulfide should be free of absorption at visible wavelengths and at 1.06 μm, and transparent throughout the infrared until the fundamental multiphonon absorption bands beginning near 10 μm are encountered. In practice, the CVD zinc sulfide prepared at Raytheon prior to this program exhibited a wide range of optical quality. The transmittance at wavelengths below 10 μm was reduced by a combination of vibrational and electronic absorptions due to impurities and deviations from stoichiometry, obscuration by particulate impurities, and scatter by pores and small particles with refractive indices different from the matrix. It was found experimentally that this attenuation could be minimized and the visible imaging quality material could be grown at low temperatures and with high excesses of zinc. The transmittance of this material is shown in Figure 4.

Our observations of the extrinsic effects in various samples of CVD zinc sulfide at both visible and infrared wavelengths can be summarized as follows:

1) In all samples grown with excess zinc there appears an absorption at wavelengths below 0.6 μm probably due to electronic transitions

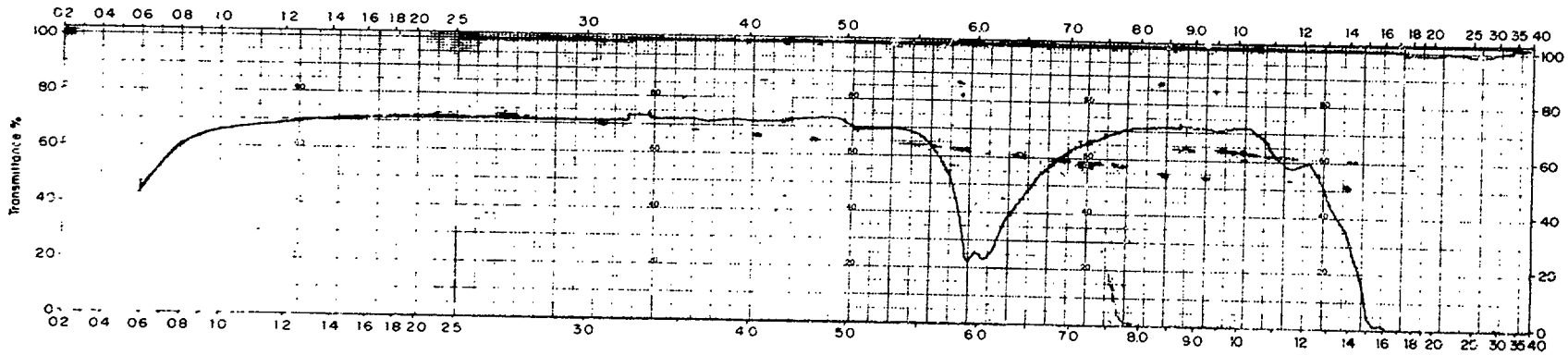

Figure 4. Transmittance as a Function of Wavelength for CVD ZnS (0.260 in. thick)

associated with sulfur vacancies. This mechanism is believed responsible for the dark coloration of CVD ZnS, but does not contribute to absorption at 1.06 μm.

2) A distinctive absorption band which is probably due to hydrogen impurities, exists primarily between 4.8 μm and 7.5 μm. This absorption has a very small, long wavelength component which contributes no greater than 0.04 cm^{-1} absorption in the range between 8.5 μm and 10 μm.

3) A wavelength independent absorption or scatter mechanism contributes between 0.04 cm^{-1} and 0.1 cm^{-1} to the attenuation coefficient at all wavelengths between 0.6 μm and 10 μm.

4) A scatter component due to small particles or pores with physical sizes in the range 200-5000 Å contributes an attenuation at wavelengths below 2 μm that shows a wavelength dependence consistent with Rayleigh-Gauss scattering.

In the past this last component has been the one most important mechanism for signal attenuation in the visible and at 1.06 μm limiting the usefulness of these zinc sulfide depositions in this spectral range. With the current technology it was possible to deposit two general types of zinc sulfide. One of the materials exhibited a relatively high percentage of small particle scatter and no wavelength independent obscuration. The other type of material had less small particle scatter (better visible range imaging) but it generally contained a few percent of wavelength independent obscuration. This second material also exhibited a deep reddish color which is attributed to sulfur vacancies. It was the goal of this phase of the program to optimize the properties of this latter type material over large plate areas, and throughout relatively thick deposits. The problem then became one of controlling the fairly well established process condition of high zinc-to-hydrogen sulfide molar ratios and low deposition temperature of 650° C.

During the course of this investigation, twenty-five (25) zinc sulfide deposition runs were made. The process conditions used in each of these runs are summarized in Table 5. Some minor modifications were made in the process conditions as the program developed, but the major development effort was devoted to testing out of several different schemes for scale-up and handling the problems encountered in the scale-up operations. It should be pointed out that the temperature and pressure control developments discussed in the sulfo-selenide work, provided improved conditions also for the zinc sulfide depositions, and this equipment was used in all of the zinc sulfide runs.

The first zinc sulfide deposition run, ZS-121P, was carried out in the seventeen-inch furnace using an 11 × 11 in. mandrel. In this deposit the mandrel plate was positioned normal to the gas flow stream, since this technique had previously been used successfully to deposit domes. Otherwise, operating conditions were similar to those developed in previous work. The visible imaging quality of this material was excellent on the edges. However, when the actual plate was polished a central core of poor imaging quality material was revealed. This section of the plate was sulfur-rich during deposition and it is known from previous work that unless the material is deposited in the presence of excess zinc the visible imaging quality of the material is poor (i. e., it exhibits high scatter). In run ZS-123P a similar mandrel geometry was used but the gas flow pattern was modified by utilizing a deflector in the center of the gas core. The deflector was effective in that the core was eliminated and the quality of the deposit across the plate was constant.

In runs ZS-124P, -125P, and -126P, a normal through-flow mandrel, as well as a mandrel perpendicular to the gas stream, was used. This was accomplished by placing the 11 X 11 in plate on top of an 8 X 10.5 in. through-flow box mandrel. In ZS-124P adjustments were made in the reactant gas flows (zinc vapor, H_2S gas) such that they entered the mandrel at equal velocities. In ZS-125P the reactant gas concentrations were reduced in order to reduce the deposition rate. In ZS-126P additional modifications were made in the gas mixing arrangements, and deposition was carried out

TABLE 5

DEPOSITION CONDITIONS

Run No.	Mandrel Temp (° C)	Furnace Pressure (torr)	Zn Retort Temp (° C)	H_2S Flow (lpm)	Deposition Time (hrs)	Zn Pickup Rate (gm/hr)
ZS-121P	660	40	645	1.15	120	---
ZS-123P	640	40	610	1.5	83	low
ZS-124P	650	40	615	2.0	110	800
ZS-125P	670	40	640	1.0	173	350
ZS-126P	665	40	620	1.25	212	280
ZS-128P	670	40	640	1.0	97	330
ZS-130P	670	40	620	1.0	224	330
ZS-133P	670	40	630	1.0	216	330
ZS-134P	645	40	635	1.5	125	515
ZS-137P	655	40	640	1.5	47	266
ZS-139P	660	40	605	1.5	56	465
ZS-140P	660	40	605/615	1.5	24/35	399/600
ZS-142P	660	40	605	1.5	118	465
ZS-143P	660	40	605	1.5	156	400
ZS-144P	610	40	630	1.5	118	400
ZS-145P	660	40	605	1.5	71	400
ZS-146P	674	30	662	3.75	67	1107
ZS-147P	660	40	602	1.5	120	425
ZS-148P	605	40	645	1.5	120	425
ZS-149P	645	40	660	2.4	200	821
ZS-150P	664	40	595	1.25	130	470
ZS-151P	610	40	630	1.25	156	425

Table 5 (Cont'd)

Run No.	Mandrel Temp (° C)	Furnace Pressure (torr)	Zn Retort Temp (° C)	H_2S Flow (lpm)	Deposition Time (hrs)	Zn Pickup Rate (gm/hr)
ZS-152P	635	40	615	1.25	142	400
ZS-156P	635	40	650	1.75	117	550
ZS-157P	630	40	645	2.4	212	960

for 212 hours. All during the deposition, temperature, pressures, flows, and zinc usage rate were held constant. The resultant deposit was very encouraging even though the thickness profile was adverse and did not yield a large area of material at the desired thickness. The optical quality was quite good and a 4-1/2 in. diameter disc, approximately 0.450 in. thick, was optically polished to specification and delivered to the project engineer. The deflector which was placed at the top of the mandrel encouraged a high growth rate in this region. That is, the deflector caused the gases to be forced towards the top third of the mandrel wall, resulting in exaggerated growth rates which normally accompany high turbulence. Even without the top gas deflector, however, the thickness distribution would have been adverse, being thin at the bottom of the mandrel due to insufficient concentration of reactants in that area. Both of these conditions suggested modifications that were incorporated into the following runs.

Based on the results of ZS-126P it was obvious that the position of the H_2S gas nozzle had to be withdrawn in order to reduce the H_2S gas velocity prior to it entering the lower part of the mandrel. The deflector at the top of the mandrel which caused the high buildup in that area was also removed since "coring" in the top plate was not a major concern because the H_2S nozzle was so low and the gases would be completely mixed by the time they reached the top of the mandrel. In order to lower the H_2S input nozzle to the desired position it was necessary to redesign the zinc retort assembly. This setup was built and used in a series of runs, ZS-128P, -130P, -133P and -134P.

In these four runs the H_2S input nozzle was raised, lowered, and otherwise modified to try to adjust the thickness profile over the plates. The optimum for this series was ZS-130P where growth was carried out for a period of 224 hours. The thickness profile for the reverse flow plate and one for the through-flow plates from this run are shown in Figures 5 and 6 respectively. As seen from these profiles, the size of a polished plate at any desired thickness is governed by the lateral thickness. It was felt that

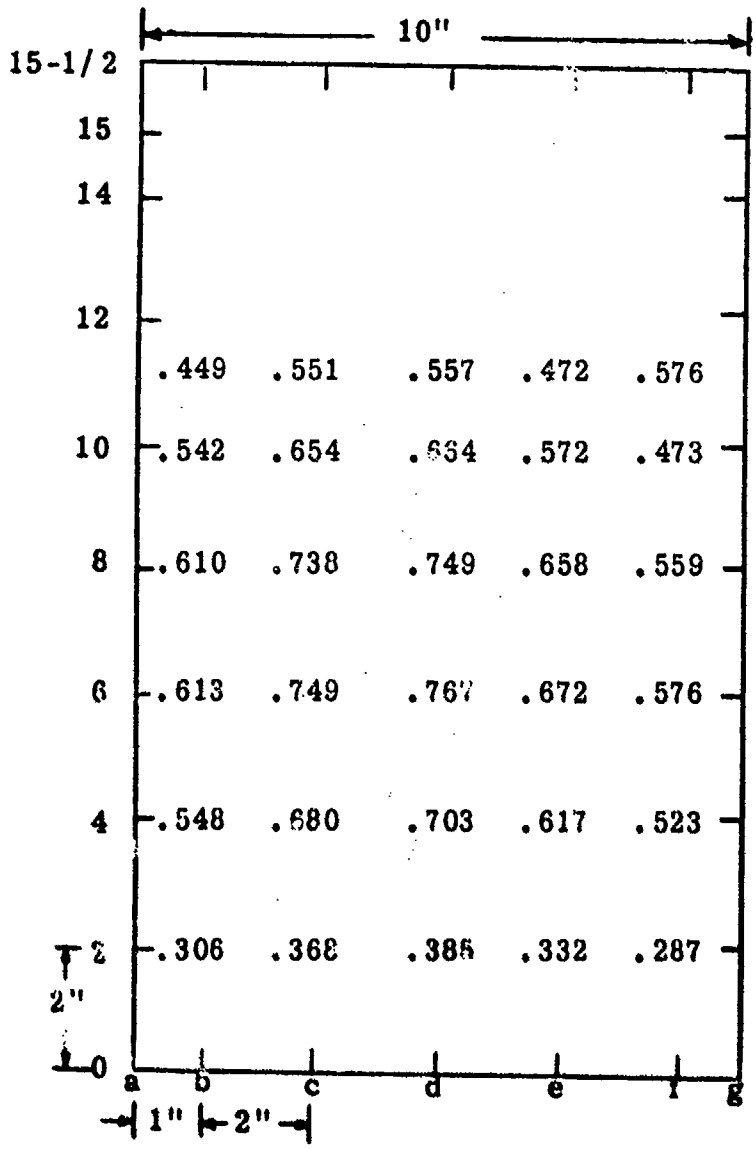

Figure 5 Thickness Profile, ZS-130P, Top Plate

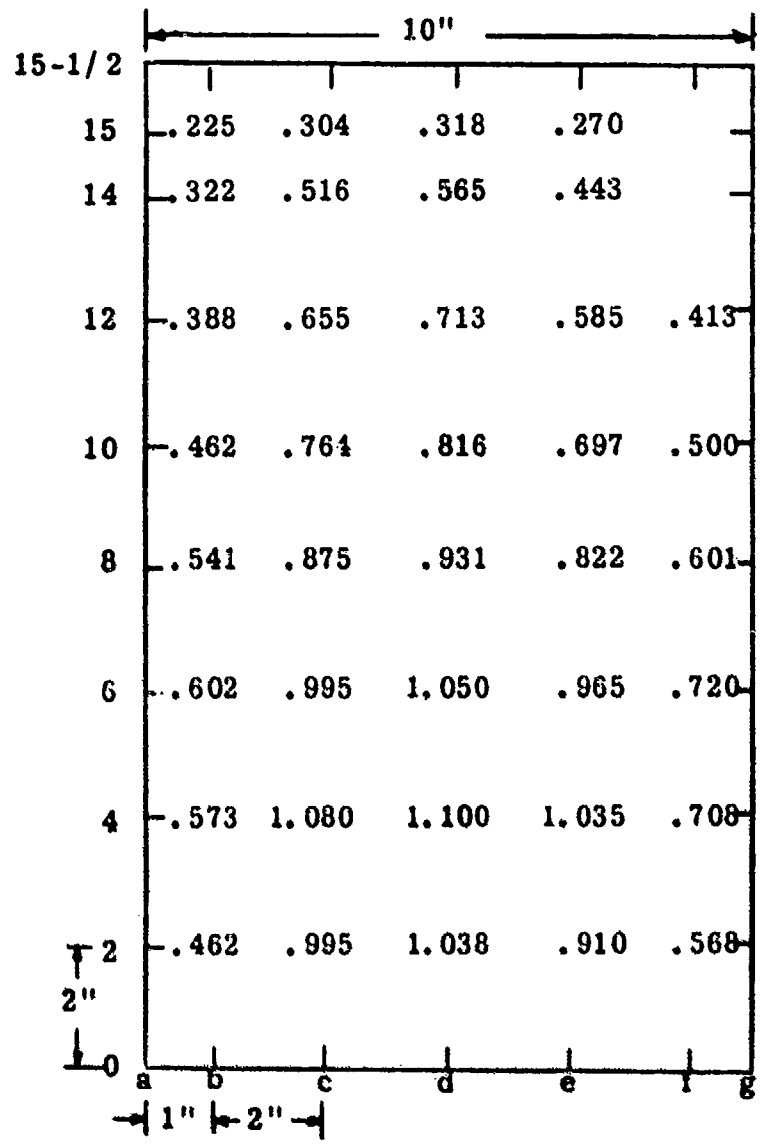

Figure 6 Thickness Profile, ZS-130P, Side Plate

this was the limit of this particular mandrel configuration and that a considerably larger sized mandrel was needed to attain a 10 × 10 × 0.625 in. plate. To accomplish the above we eliminated one of the mandrel plates, and thus optimized the available furnace area with one plate at the center of the furnace diameter. A completely new retort and mandrel setup was designed and built using this new single mandrel plate concept. The new setup incorporated all of the positive innovations we had made in the H_2S and zinc vapor flow pattern control in previous runs. Some modifications were also made in the exhaust section which we hoped would accommodate more of the excess zinc than previous designs. A series of eleven (11) runs were carried out in this setup.

The first three of these runs, ZS-137P, -139P, and -140P, were process runs, all less than 60 hours duration, to try to evaluate the new mandrel configuration. Again, modifications were made in the gas flow and mixing arrangements to optimize deposition rate and thickness profile. These runs were encouraging in that deposition proceeded in a uniform manner for the 60 hour period. The thickness profile of ZS-140P, for example, is given in Figure 7. The optical quality and visible imaging quality of two witness samples taken from this plate were excellent. Two-inch diameter witness samples were cut from two sections of the plate (designated in Figure 7) and delivered to the project engineer.

In runs ZS-143P, -144P, -145P, -147P, -148P, -150P and -151P we attempted to deposit the 5/8 in. thick plate but did not succeed. In the first few full deposition period runs we experienced clogging in the exhaust end of the mandrel that was caused by condensation of the large volumes of excess zinc. In the latter runs the clogging problem was finally solved by reducing total flow of all the reacting species. This, however, adversely affected the growth rates and rendered this approach impractical for producing the desired finished plate.

It was concluded at this time that in order to increase the growth rate in the runs in the 17-inch furnace the mandrel configuration would have

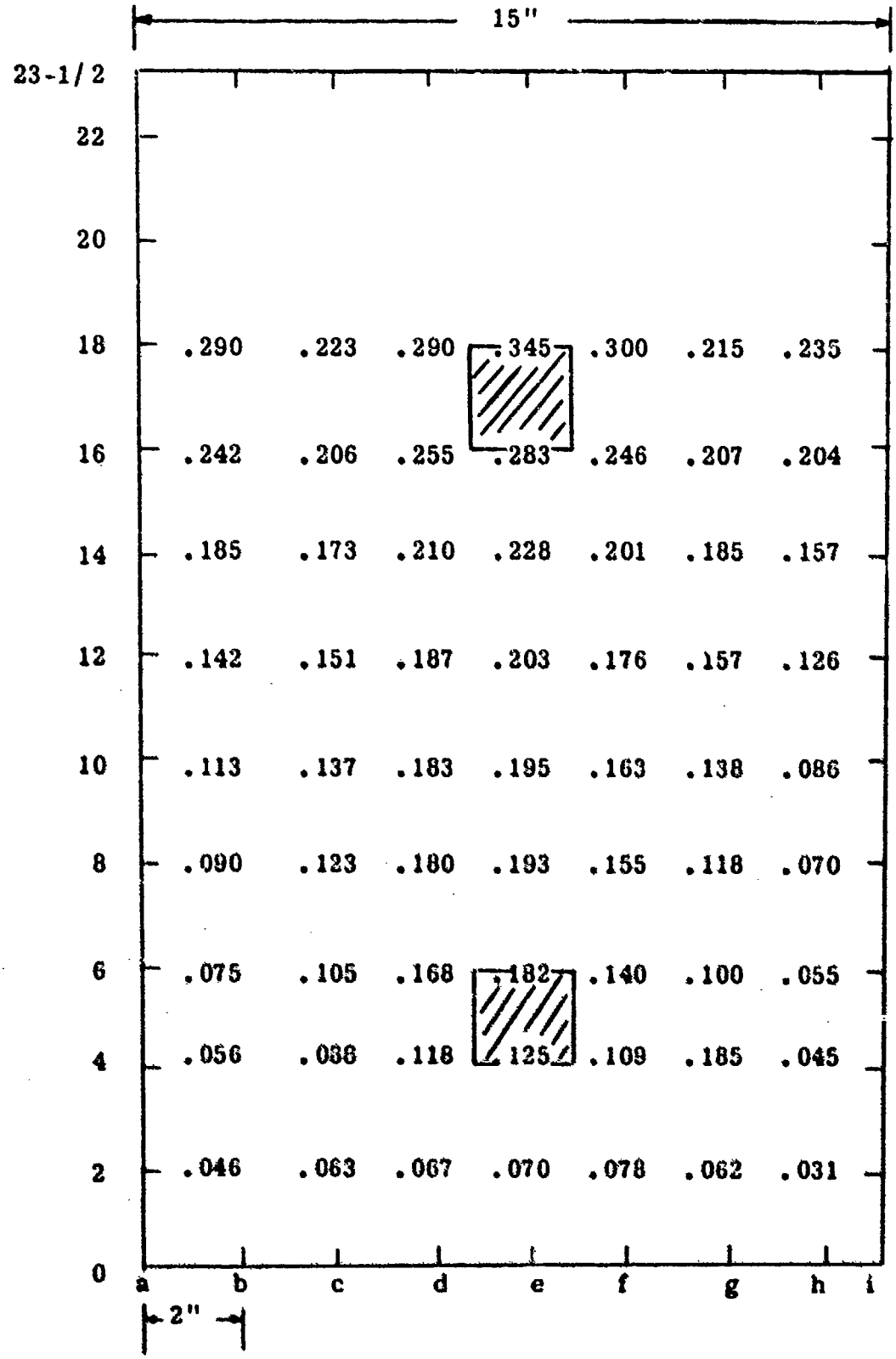

Figure 7 Thickness Profile, ZS-140P and Location of Witness Samples

to again be changed. Two runs ZS-152P and -156P, were made using a 5-inch by 14-inch rectangular cross-section mandrel that was 20 inches long. The gas input and mixing chamber configurations were not changed from those used in the previous setup. Both ZS-152P and -156P the only runs in this new mandrel, were quite successful. Deposition was carried out for over 140 hours and 117 hours respectively before exhaust clogging forced termination. Plates 20 X 14 in. resulted from these runs which were just slightly below the required 5/8 in. thickness over a 10-inch by 10-inch area. The thickness profile of one of the plates from ZS-152P is shown in Figure 8. The visible imaging quality and the transmission at 1.06 μm measured on samples from these runs were excellent.

It was obviously desirable to have room for a longer gas mixing area and have a larger exhaust area than was possible to achieve in the 17-inch diameter furnace. Therefore a much larger furnace (52-inch diameter) was used to make the next series of runs.

ZS-146P was the first zinc sulfide deposit carried out in the large 52-inch diameter furnace. For this run a 34 X 17 X 9 in. rectangular box mandrel was used. Deposition of ZS-146P was carried out for 67 hours. In the beginning of the run some difficulty was experienced in attaining the high zinc pickup rate needed to deposit high optical quality material. As a result, it was necessary to increase the deposition temperature and to slightly reduce the furnace pressure. These changes resulted in the desired zinc pickup rate but adversely affected optical quality of the material. Overall, the run was considered quite successful. The transverse thickness profile was quite good. Axially, however, the thickness profile needed improvement. The optical quality of the material, because of the higher deposition temperature, was not equivalent to our normal material.

The next run made in the 52-inch diameter furnace was ZS-149P. In this run the retorts were modified so that the desired zinc usage rate could be obtained when the mandrel temperature was 645° C. The H_2S flow rate was lowered to obtain the required H_2S:Zn partial pressures in the

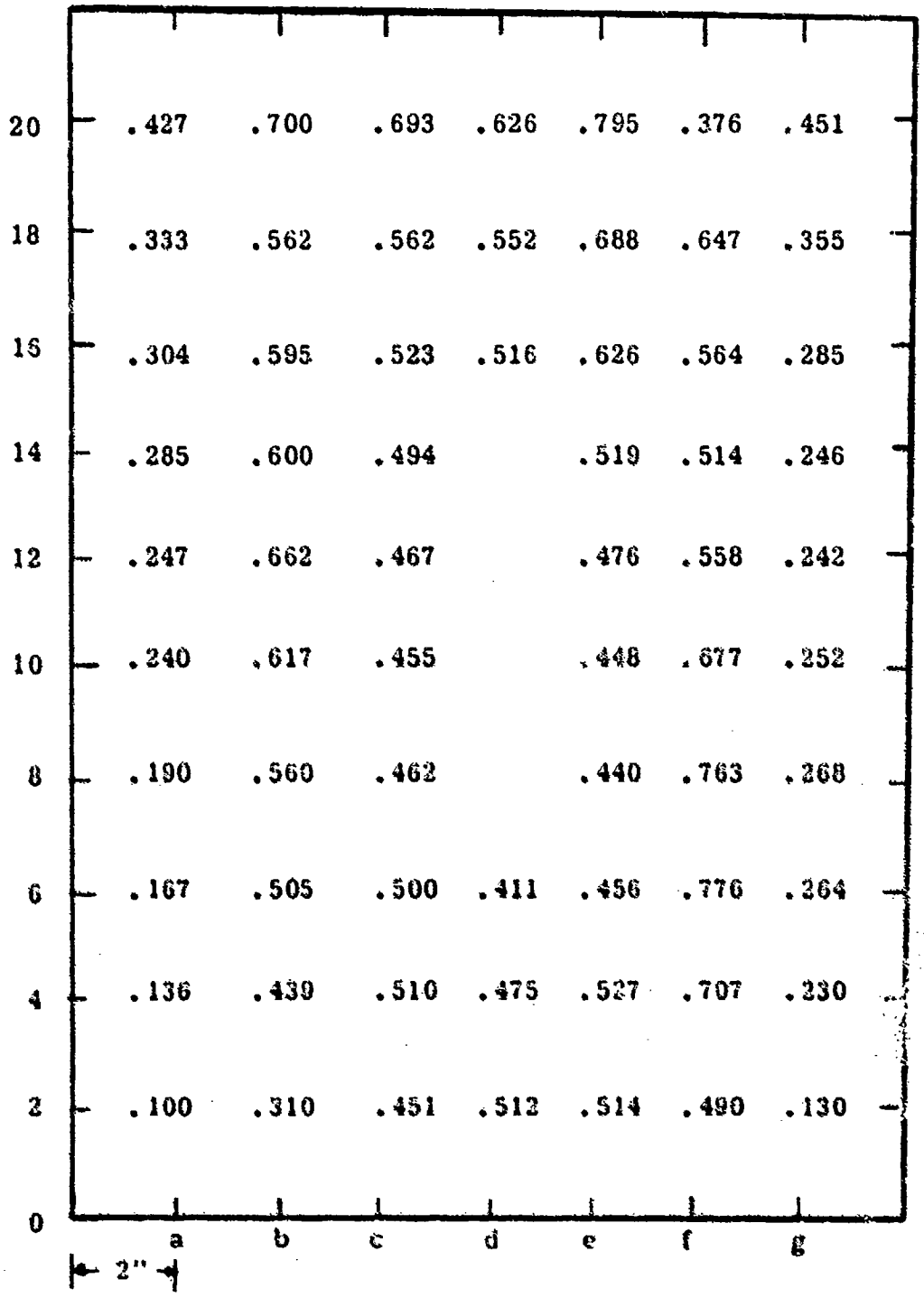

Figure 8. Thickness Profile, ZS-152P, Plate C

mandrel area. No modifications were made in any of the exhaust ports since there were no indications of clogging in ZS-146P. Deposition was carried out for 200 hours with constant run conditions, i.e., temperature, pressure, zinc pickup, etc. The resultant material from this run was quite good, although the thickness profile was not as good as desired. It was obvious from the top heavy profile that further adjustments were needed to increase the deposition rate on the lower half of the mandrel. The visible imaging quality of this deposit was good, especially at the center area where the finished part would be located.

In the final run, ZS-157P, several modifications were made to the flow geometries used in ZS-149P so that the thickness profile would be improved. This run was successfully completed after 212 hours of continuous deposition. All temperature, pressure, and other control systems functioned properly throughout the entire deposition period. Two plates, 17 × 34 in., were produced. Figure 9 shows the thickness profile of one of the 17 × 34 in. plates, while Figure 10 shows the location of the 10 × 10 in. blank. This plate was sent out for grinding and polishing to the required 0.625 in. thickness and subsequent imaging spoiling measurements. A second test piece 6 inches in diameter, which was used for MTF optical testing, was also cut out as indicated in Figure 10.

The image spoiling measurements were performed at the Air Force Avionics Laboratory on the 10 inch square blank. Basically, the measurement consists of measuring the width of the image of a line source (slit) formed by a high quality imaging system, and then noting the increase in the image width resulting from insertion of the window blank at an appropriate place in the optical path. An image spoiling value of about 6 microradians was observed in the 7 to 12 μm region. This is considered an excellent value.

Measurement of the modulation transfer function (MTF) were made by Texas Instruments Image Evaluation Laboratory on the 6-inch diameter disc. With the aid of a 36-inch focal length off-axis parabola, the MTF

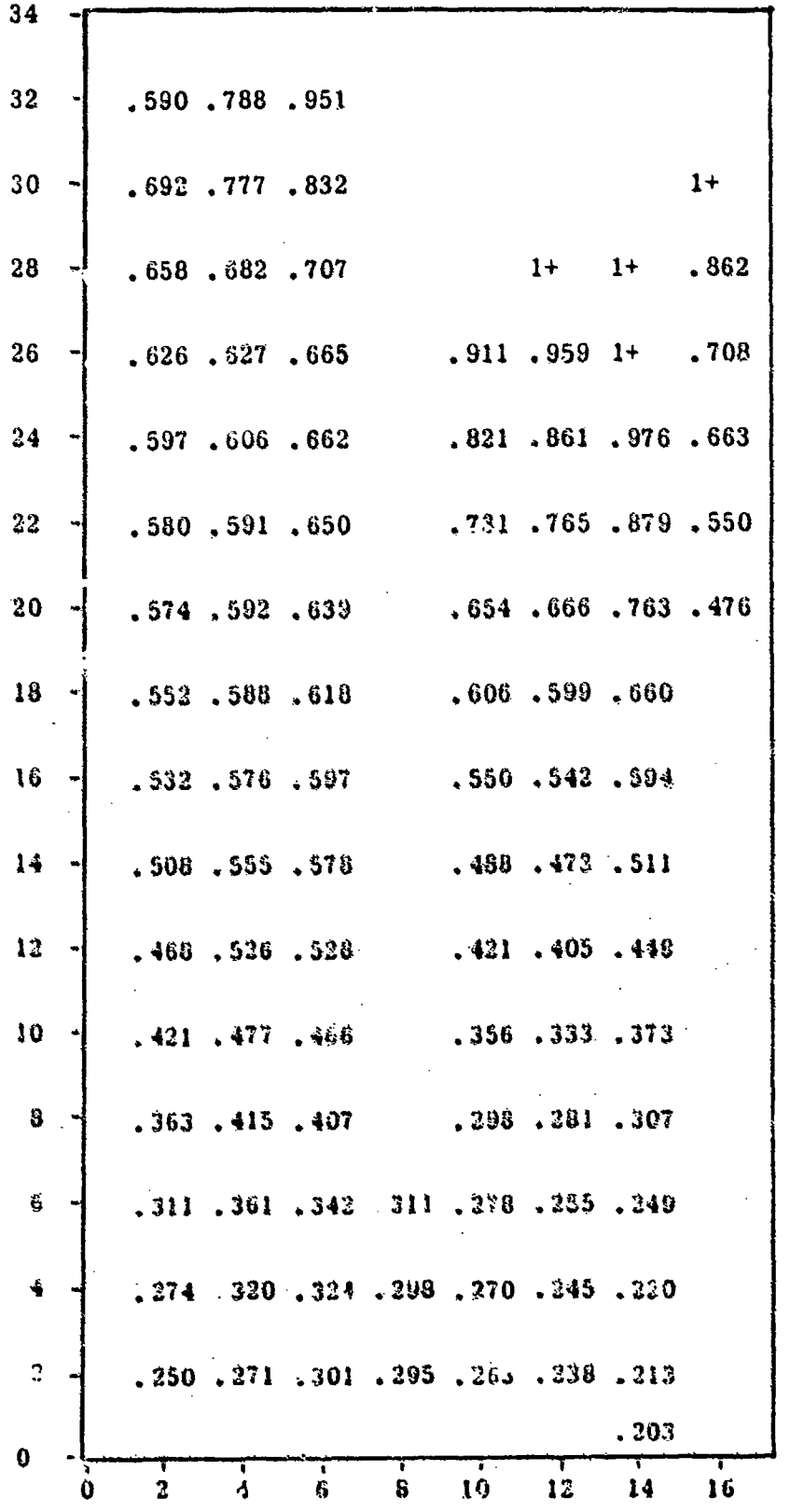

Figure 9 Thickness Profile of Plate A, Run Z5-157P

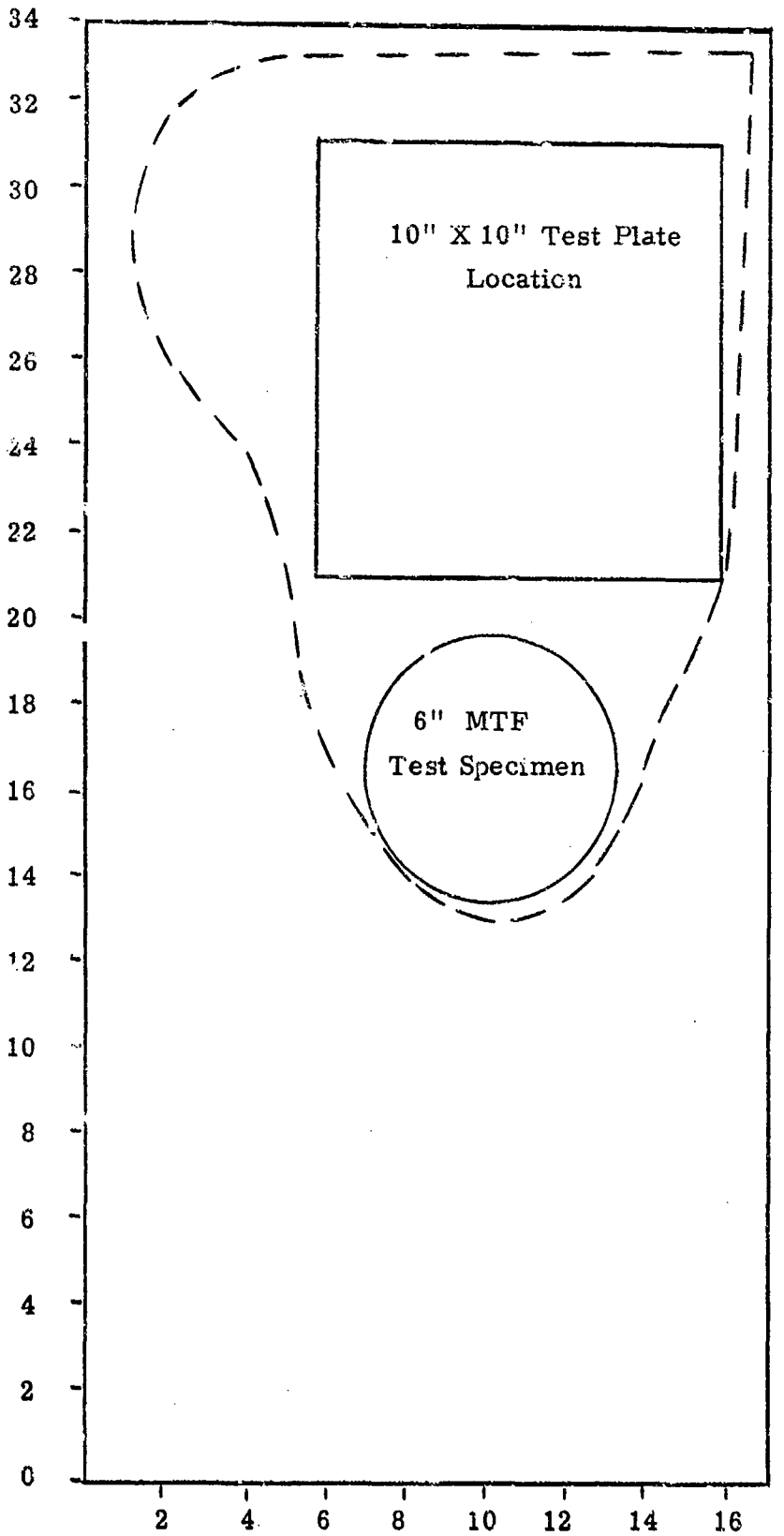

Note: Area inside dotted line cleared rough polish at 0.625"

Figure 10 Sample Locations from Plate A, ZS-157P

was measured for a spatial frequency of 5.5 line pairs/ mm (corresponding to 5 cycles/ milliradian). For the 8 to 12 μm spectral region the MTF was 98.3% and 97.6% for two orientations of the blank, differing by a 90° rotation about the blank axis. At 1.06 μm the MTF values for two orientations were 98.7% and 98.8%.

The spatial frequency of 5.5 lp/ mm means that a single line subtends an angle of 100 microradians at the parabola. The very high values of MTF thus indicate that the spreading caused by the window blank is much less than 100 microradians, which is consistent with the results of the image spoiling measurements.

The visible imaging quality of test samples taken from this run (ZS-157P) was excellent. The transmission from 0.2 to 14 μm for a polished sample 0.6 inch thick is shown in Figure 11. The deep absorption band at 6 μm, which is accompanied by some shallower absorptions at approximately 4 μm and 5 μm, is the characteristic absorptions which are observed in runs where very high zinc ratios are used. It is also noteworthy that the uncoated transmission at 1.06 μm for this thickness sample was approximately 50 percent.

Hardness tests on samples from ZS-157P showed a hardness, $K_{50} = 216$. This is consistent with values for previous CVD zinc sulfide samples deposited under similar conditions. A set of twenty (20) flexural strength beams (0.200 × 0.250 × 3.0 in.) representative of the 10 × 10 in. plate, were prepared and tested in four-point loading over a 1 in. span. The average strength determined from these measurements was greater than 19,000 psi as shown from the results

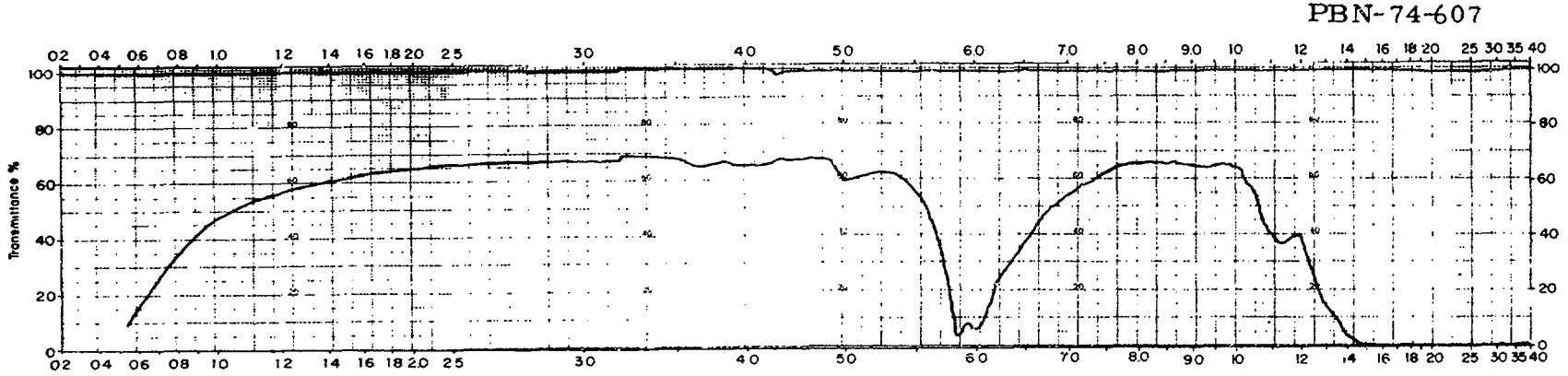

Figure 11. In-Line Transmission, Run ZS-157P, Thickness = 0.600 in. (Side Plate)

that are tabulated in Table 6. These strength values are representative of our highest quality, fine-grain material.

The 10 × 10 × 5/8 in. plate, along with the 6-inch diameter disc, indicated in Figure 10, were polished at Group 128 Inc., Waltham, Mass. to the following specifications:

a) Parallelism of optical faces: 0° 0" 45" + 24" - 0"

b) Sphericity of surfaces: < 2 fringes (helium light) over any 5-inch diameter

c) Surface irregularities: < 1/4 fringe (helium light) over any 5-inch diameter

d) Surface finish: Fine ground. Edges chamfered 45°, 80-50 scratch and dig (MIL-O-13830) with no visible grayness.

The 10 × 10 inch plate (shown in Figure 12) was submitted to the project engineer on September 6, 1974.

3.4 Zinc Sulfide Domes

The third goal of this program was to develop process conditions and to fabricate a zinc sulfide hemispherical dome 9 inches in diameter which will have sufficiently wide spectral transmission to allow multispectral service from the visible out to the multiphonon region. The dome development work was aided immeasurably by the intensive development work on large zinc sulfide plates and sulfo-selenide. In addition, the dome thickness requirements for anticipated zinc sulfide dome applications was 1/4 in. which eliminated the need for long duration deposition and the clogging, problems encountered in the large zinc sulfide plate depositions. As a result, progress on dome development went along smoothly and a high quality dome was produced

TABLE 6

ROOM TEMP FLEXURAL STRENGTH OF ZS-157P

Deposition Samples		σ (psi)
1		19,395
2		19,861
3		14,859*
4		21,695
5		16,242
6		16,621
7		20,119
8		15,270*
9		10,768*
10		20,232
	Avg. of 7	19,166 ± 1,852

Substrate Samples		σ (psi)
1		18,984
2		17,088*
3		19,878
4		15,646*
5		18,583
6		22,644
7		19,464
8		19,125
9		19,657
10		19,726
	Avg. of 8	19,757 ± 1,163

*Early failure may be due to surface flaws

Figure 12. Zinc Sulfide Plate From Run ZS-157P, Optically Polished and Ready for Delivery, 10 × 10 × 5/8 in.

in the sixth deposition. There were seven dome depositions carried out altogether, the seventh being a multiple dome deposition attempt. Process conditions for each of these runs are reported in Table 7. The process conditions evolved from the plate development work and were not altered appreciably in the dome deposition. Attention was focussed on modifications in the mandrel assembly which would allow constant thickness deposition over a hemispherical shape.

In the first zinc sulfide dome deposition, ZS-1-D, a 2.87 inch radius spherical dome mandrel was used. A direct flow setup was used where the female graphite dome mandrel was mounted normal to the input gas flows as in the inverted plate setup previously described. Deposition was carried out for 50 hours under well controlled process conditions. The resultant dome was 1/4 to 3/8 in. thick with the thickest section being the center of the dome. The optical quality of this dome varied over the dome surface with the center region having the worst optical quality (i.e., higher scattering). This is as one would expect considering a core of H_2S gas impinging on the central part of the dome resulting from the high sulfur partial pressure in that region.

With the successful deposition of the small dome, a 9-inch diameter hemispherical dome was deposited in the second run, ZS-2-D. The mandrel configuration for this run was essentially the equivalent to ZS-1-D except for the larger diameter mandrel. Deposition for this run was also carried out for 50 hours. The sides of this dome were of excellent optical quality but there still was a core of high scattering material at the center of the dome where the H_2S concentration was highest.

In ZS-3-D a deflector similar to that used in the 11 × 11 in. plate mandrel was suspended below the dome mandrel in order to breakup and deflect the H_2S flow and consequently eliminate the core. Other than for the use of the deflector, this run was similar to ZS-2-D with the 9-inch diameter dome mandrel. Deposition in this run was carried out for 60 hours because it was felt that the deflector would result in a lower deposition rate

TABLE 7

DEPOSITION CONDITIONS

Run No.	Mandrel Temp (° C)	Furnace Pressure (torr)	Zn Retort Temp (° C)	H_2S Flow (lpm)	Deposition Time (hrs)	Zn Pickup Rate (gm/hr)
ZS-1-D	660	40	635	1.5	50	400
ZS-2-D	670	40	650	1.5	50	450
ZS-3-D	600	40	634	1.5	60	420
ZS-4-D	660	40	645	1.5	29	400
ZS-5-D	640	40	650	1.5	35	525
ZS-6-D	640	40	630	1.5	69	525
ZS-7-MD	640	40	640	1.7	60	525

on the mandrel. The resultant dome from this run was a complete hemisphere and the entire area of the hemisphere was of excellent optical quality. The deflector eliminated the core problem and thickness profile problems completely. Cracking of the dome during polishing, however, rendered dome ZS-3-D useless as a deliverable end item. Two more runs, ZS-4-D and ZS-5-D, were carried out with slight modification in temperature profile to resolve the cracking problem.

The next dome deposit, ZS-6-D, duplicated the process conditions for ZS-5-D except that deposition was carried out for 69 hours. The 9-inch diameter dome setup was again used with no modifications. Full temperature and pressure control was employed throughout the entire deposition period. The resultant dome, ZS-6-D, was again a full hemisphere with a nominal 1/4 inch wall thickness. The thickness profile as measured at several latitudes on the hemisphere is shown in Figure 13. The measurements show that the overall thickness profile is $\pm$ 15 percent. We also measured the radius of the deposited dome using a 3-inch spherometer. The average radius measured was 4.53 in. which allowed 0.030 in. for grinding and polishing to a final specified radius of 4.500 $\pm$ 0.005 in.

The optical transmission from 0.2 to 40 μm of a witness sample from this run is shown in Figure 14. The transmission data show greater than 60 percent transmission at the critical 1.06 μm wavelength. In addition, resolution of transmitted visible range images was excellent. The 8 μm to 10.6 μm wavelength transmission is approximately seventy (70) percent.

The dome from ZS-6-D was cut off at a full 180° hemisphere. The as-grown cutoff hemisphere is shown in Figure 15 along with the uncut dome from ZS-5-D. The 180° segment from ZS-6-D was final ground and polished at Penn Optics, Reading, Pa. to the following specifications:

a) Surface: 80-50 scratch-dig with no visible greyness

b) Wall thickness: 0.17 in. $\pm$ 0.001

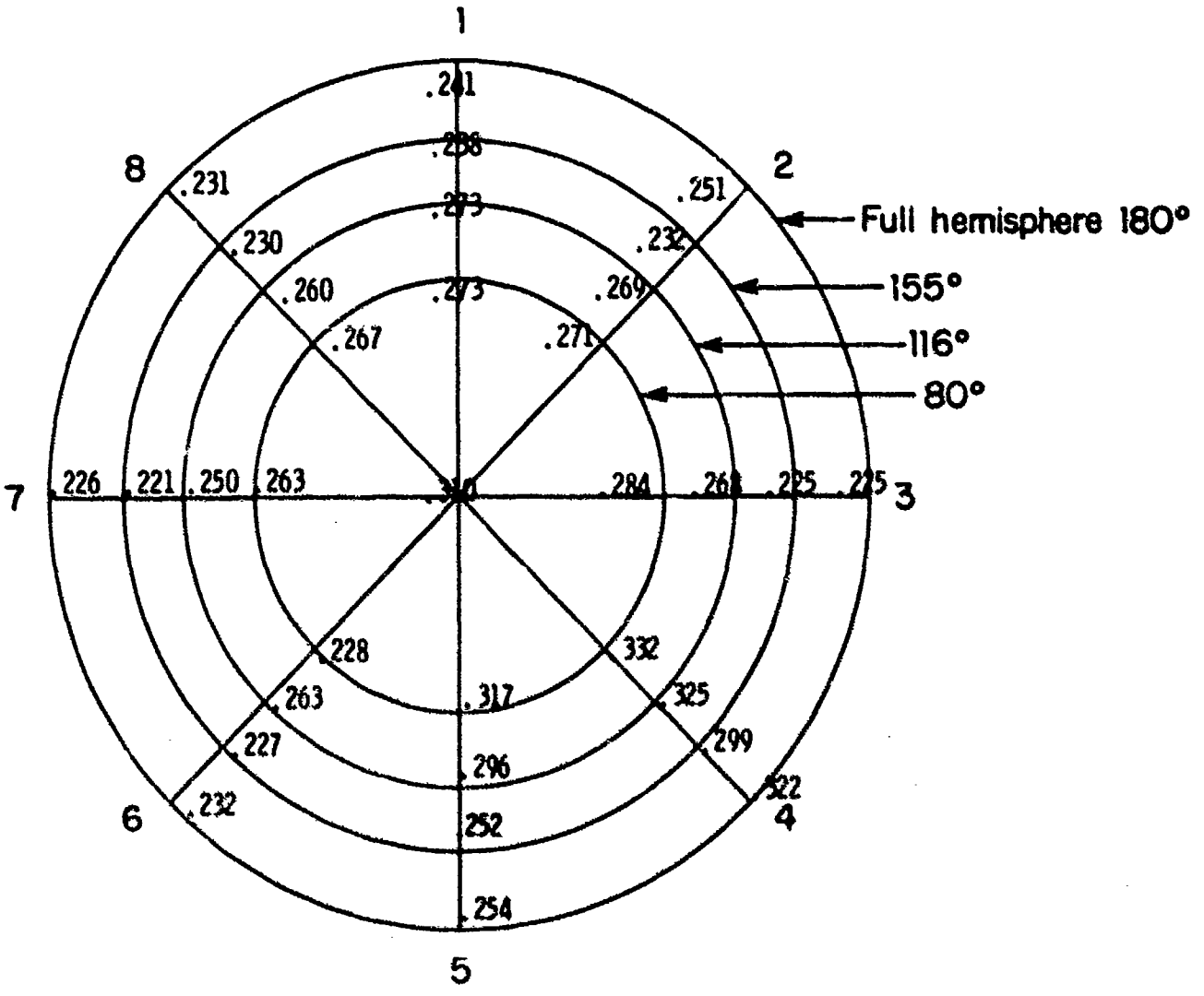

Figure 13 Thickness Profile of Zinc Sulfide 9-Inch Diameter Dome, ZS-6-D

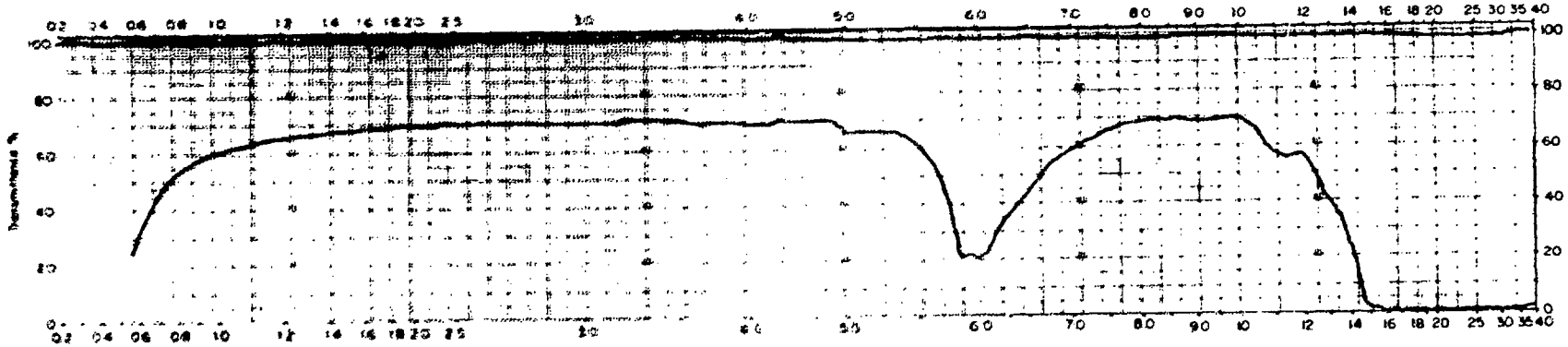

Figure 14. In-Line Transmission, Zinc Sulfide Dome ZS-163-D, t = 0.195 in. (Dome Support Ring)

Figure 15. Hemispherical Domes ZS-5-D and ZS-6-D With ZS-6-D Shown Cut Off at 180° Prior to Submission for Optical Polishing

c) Convex radius: 4.500 in., 5 ring power match to a 2-inch test glass
1 ring regularity to a 2-inch test glass

d) Concave radius: 4.327 in., 5 ring power match to a 2-in. test glass
1 ring regularity to a 2-in. test glass

e) Optical performance: 96% efficiency per any 1-1/2 in. dia. of the dome when checked by the K. D. C. test described in MIL handbook 141.

The finished dome, shown in Figure 16, was submitted to the project engineer.

In order to make the dome depositions more practical it is necessary to deposit more than one dome segment at a time. This requires that the domes be deposited on side walls in a through-flow configuration rather than the reverse flow configurations. We therefore designed and evaluated a setup to deposit four (4) dome segments simultaneously. Each dome segment was 9 in. in diameter but they were not full 180° segments due to the anticipated difficulty of maintaining a constant deposition thickness profile in deep horizontal recessions using the through-flow configuration. A 60-hour deposition was carried out (ZS-7-MD) using this setup.

This feasibility attempt to deposit more than one dome segment at a time was extremely successful. All four dome segments were uncracked and of excellent optical quality. The thickness profile of each dome was better than anticipated. We are confident that with further development multi-dome deposits can be successfully made and that the costs of a dome can be significantly reduced.

3.5 Zinc Sulfide Surface Coating

One of the requirements of a multispectral window is that it withstand airborne environmental conditions. The severest of these requirements is rain erosion resistance wherein the window is required to withstand impact

Figure 16. Ground and Polished 9-Inch Diameter Zinc Sulfide Dome, ZS-6-D.

of water droplets at high speeds. To meet this requirement with brittle materials, in general the hardest material available is chosen. In the case of zinc sulfide, this material would be deposited at 650° C.

Evaluation of rain erosion failures in test samples of zinc sulfide and sulfo-selenide solid solution reveals the presence of concentric ring cracks that are all approximately of equal size and that penetrate into the sample about the same distance (~ 1/2 mm). These concentric ring cracks suggest tensile failure of the material due to compression of the material under the area of impact. These failures also suggest that if the surface of a material were placed in compression that higher impact loads would have to be applied before failure occurred. One method of accomplishing the above would be to deposit thin layers of zinc sulfide onto zinc selenide. Because of the different thermal expansion coefficients of the sulfide and the selenide the surface sulfide layer would be placed into compression.

Three runs were carried out to evaluate the feasibility of this approach. The process conditions for these runs are summarized in Table 8. Initially it was necessary to establish whether the deposition could be switched from zinc selenide to zinc sulfide abruptly and still maintain the continuity of the deposit. In run ZS-Se-C-1 zinc sulfo-selenide was deposited for an initial 12 hours. The run was continued with only H_2S gas for a final 5 hour deposition period. This resulted in approximately 20 mils of ZnS on the surface of the deposit. Photomicrographs of a cross-section of the solid solution-to-zinc sulfide interface (Figure 17) clearly show the two regions. It is also important to note that individual grains are continued across the interface. This run, therefore, established the feasibility of depositing sound surface layers and led to two additional runs. Both of these runs started out with a period of ZnS growth which was then gradually graded into ZnSe for a total of over 200 mils of growth.

In ZS-Se-C-2 pure zinc sulfide was deposited for five hours. For the next eight hours the H_2S input was substituted with H_2Se gas in eight, one-hour steps. Finally, for a period of sixty hours pure zinc selenide was

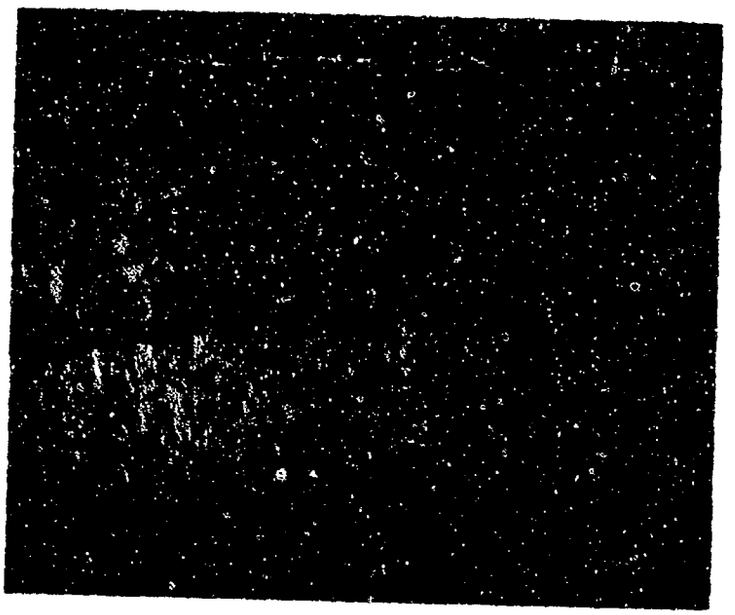

Figure 17. Interface Region of ZnS Layer Grown Onto Zinc Sulfo-Selenide

TABLE 8

DEPOSITION CONDITIONS

Run No.	Mandrel Temp (° C)	Furnace Pressure (torr)	Zn Retort Temp (° C)	H_2S Flow (lpm)	H_2S Hrs	Composition Gradient Flow (lpm)	Composition Gradient Hrs	H_2Se Flow (lpm)	H_2Se Hrs	Zn Pickup Rate (gm/hr)
ZS-ZSe-C1	700	60	595	0.5	5	---	---	0.5	12	80
ZS-ZSe-C2	700	40	590	0.5	5	8 steps	8	0.5	50	75
ZS-ZSe-C3	700	40	590	0.5	5	16 steps	8	0.5	70	75

deposited. Cross-sectional views of the resultant deposit showed individual bands corresponding to each one-hour input gas composition shift. The samples showed no evidence of cracking and the adjacent layers of graded composition were intimately bonded. By viewing the sample under cross polarizers, birefrigence can be observed near one surface indicating the presence of a stressed layer as anticipated from the differences in the thermal expansion coefficients of ZnS, ZnSe and their solid solutions.

In ZS-ZSe-C-3 the conditions of ZS-ZSe-2 were repeated except that during the grading sequence, sixteen half-hour steps were used in order to reduce the banding caused by the index shifts that accompany the composition changes. Again the cross-sections showed sixteen individual bands corresponding to each composition shift.

Both of these runs yielded sufficient material for the fabrication of a number of rain erosion test samples. Samples were cut and fabricated from each of these runs, and shipped to the project engineer for testing. Figure 18 is the thickness profile of a cross-section of ZS-ZSe-C-2 showing the thickness of each composition band starting with pure zinc sulfide through to the pure zinc selenide. Using this profile the following type of erosion samples were prepared: One set with a zinc sulfide surface, one set with a high percentage sulfide solid solution surface, and one set with a low sulfide solid solution surface. This was accomplished by polishing back to the desired position as indicated in Figure 18. A similar series of three sets of samples was prepared from ZS-ZSe-C-3. Thus three degrees of surface compression were realized from each run.

Bend tests were performed on test beams from both of these runs using four-point loading over a 2-inch span. For ZS-ZSe-C-2, seven (7) beams were tested with the zinc sulfide compression layer loaded in tension, and seven (7) beams were tested with the zinc sulfide compression layer loaded in compression. All beams were approximately 0.25×0.125 in. in cross-section, and were long enough to be tested over a 2-inch span. The results of these tests are given in Table 9.

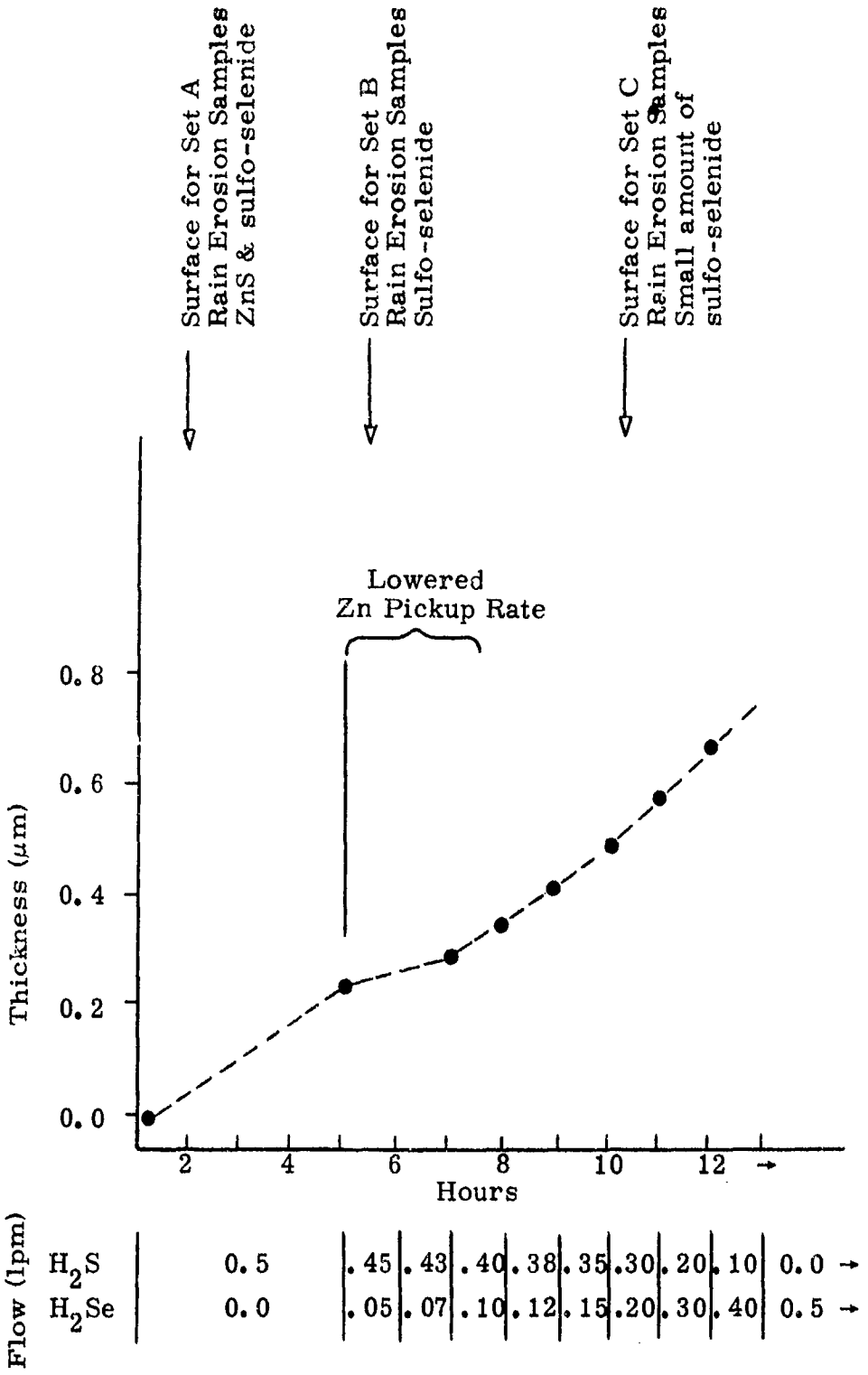

Figure 18. Thickness Profile for Graded Zone for Surface Layers on ZS-ZSe-C-2

TABLE 9

ROOM TEMPERATURE FLEXURAL TESTING OF ZS-ZSe-2-C

Sample No.	ZnS Compression Surface Loaded in Compression (psi)
1	9,641
2	9,969
3	9,259
4	9.986
5	7,749
6	11,192
7	8,948
Avg.	9,535 ± 982

	ZnS Compression Surface Loaded in Tension (psi)
1	14,112
2	12,990
3	10,632
4	12,383
5	12,921
6	15,474
7	14,393
Avg.	13,272 ± 1453

Similarly, a series of flexural beams, 0.25 × 0.125 × 3 in., from ZS-ZSe-C-3 were tested. Six samples were tested with the zinc sulfide surface in tension and six bars were tested with the zinc selenide surface in tension. We also tested a series of twelve (12) pure zinc selenide bars from the same run for comparison purposes. These test results are reported in Table 10. It is evident from the strength data for both runs that the strengths of the beams tested with the pre-stressed ZnS layer in tension are approximately 30 percent higher than when pure zinc selenide is in tension. It remains to be seen, however, whether or not the pre-stressed material results in improved rain erosion resistance.

3.6 Microstructure Analysis

The development of CVD zinc sulfide and zinc sulfo-selenide as a multispectral window has been hindered by small particle scatter. This has been the primary concern of material quality improvement efforts particularly in the visible end of the spectrum. In order to make meaningful process adjustments to eliminate or reduce the concentration of the scattering particles it became imperative to identify the makeup of the individual scatter sites. The two types of scatter sites which one would have reason to suspect could be incorporated in these deposits are: 1) micro pores, or 2) small particles of slightly different refractive index than the matrix (i.e., hexagonal zinc sulfide). Considerable effort was spent in examining the microstructure of the deposits made throughout this program in an attempt to isolate the scattering particles.

The microstructure of a number of polished and etched cross-sections were examined in a high resolution metallograph. There were obvious grain size variations from sample to sample. In addition the photomicrographs showed nodule development and maintenance as well as other unusual features. Among these are: 1) "blotches" which appear to be regions of very dense, fine-grained material, 2) crystallites which have light and dark parallel bands which are believed to be twins, and 3) an occasional needle-like structure amid other finer grained material. Figure 19 is a composite photomicrograph

TABLE 10

ROOM TEMPERATURE FLEXURAL TEST RESULTS FOR ZS-ZSe-3-C

Sample No.	Strength (psi)	
1	9,924	
2	9,735	
3	8,811	ZnSe surface loaded
4	9,437	in tension
5	9,849	
6	8,031*	
	9,551 ± 406	avg. of 5 samples
7	13,945	
8	13,754	
9	14,327	ZnS surface coat
10	13,335	loaded in tension
11	8,771*	
12	12,563	
	13,585 ± 603	avg. of 5 samples
13	5,955*	
14	9,805	
15	7,720	
16	7,253	
17	9,118	All ZnSe portion of
18	7,139	deposits
19	7,940	
20	9,142	
21	7,124	
22	8,522	
23	8,634	
24	9,493	
	8,354 ± 927	avg. of 11 samples

*Surface flaw on sample.

Figure 19. Microstructure of ZSS-32 Showing Incorporation of Needle-like Crystallites

of the entire cross-section from one of the zinc sulfo-selenide deposits. In this figure the large needles are clearly visible and are contrasted to the smaller grain size matrix material. This is a dramatic representation of the fact that there are different modes of crystallization and that the scatter sites could be associated with these microstructural inconsistencies.

During one of the earlier zinc sulfo-selenide depositions the temperature inadvertently rose 50° to 100° C for a short period of time. The deposited material before and after the temperature rise showed powder-like inclusions, while the high temperature region was clear. We attempted to identify the cause of the "cloudy" regions by microprobe profile analysis. Figure 20 shows the relative intensities of the zinc, selenium, and sulfur concentrations of one traverse across the sample. These traces show an obvious solid solution composition change in the clear region which would cause an index change and banding. There is, however, no obvious identification of the scatter sites causing the cloudy appearance.

X-ray powder diffraction investigations on these materials has shown that the zinc sulfide phase is not completely cubic, but also contains a small amount of a hexagonal phase. This is discernible from the shape of the (111) cubic diffraction peak that is broad and suggestive of a wide polytype distribution. It was estimated from the relative intensity of these diffraction peaks that if the broadness was due to the presence of a hexagonal phase it represented less than 2 percent of the deposit. Even this amount of inclusion of a second phase having a $\Delta n \sim 2 \times 10^{-3}$ can cause severe image distortion depending on the particle size.

It is also well known that the c-axis of the hexagonal phase and the (111) direction of the cubic phases of zinc sulfide are common axes. In fact, it is not difficult to imagine the stacking sequence shifting back and forth from an ABAB... hexagonal stacking to an ABC ABC ... cubic stacking during deposition. In addition, one can imagine almost any size region of one modification expitaxially depositing on the other resulting in individual

PBN-73-964

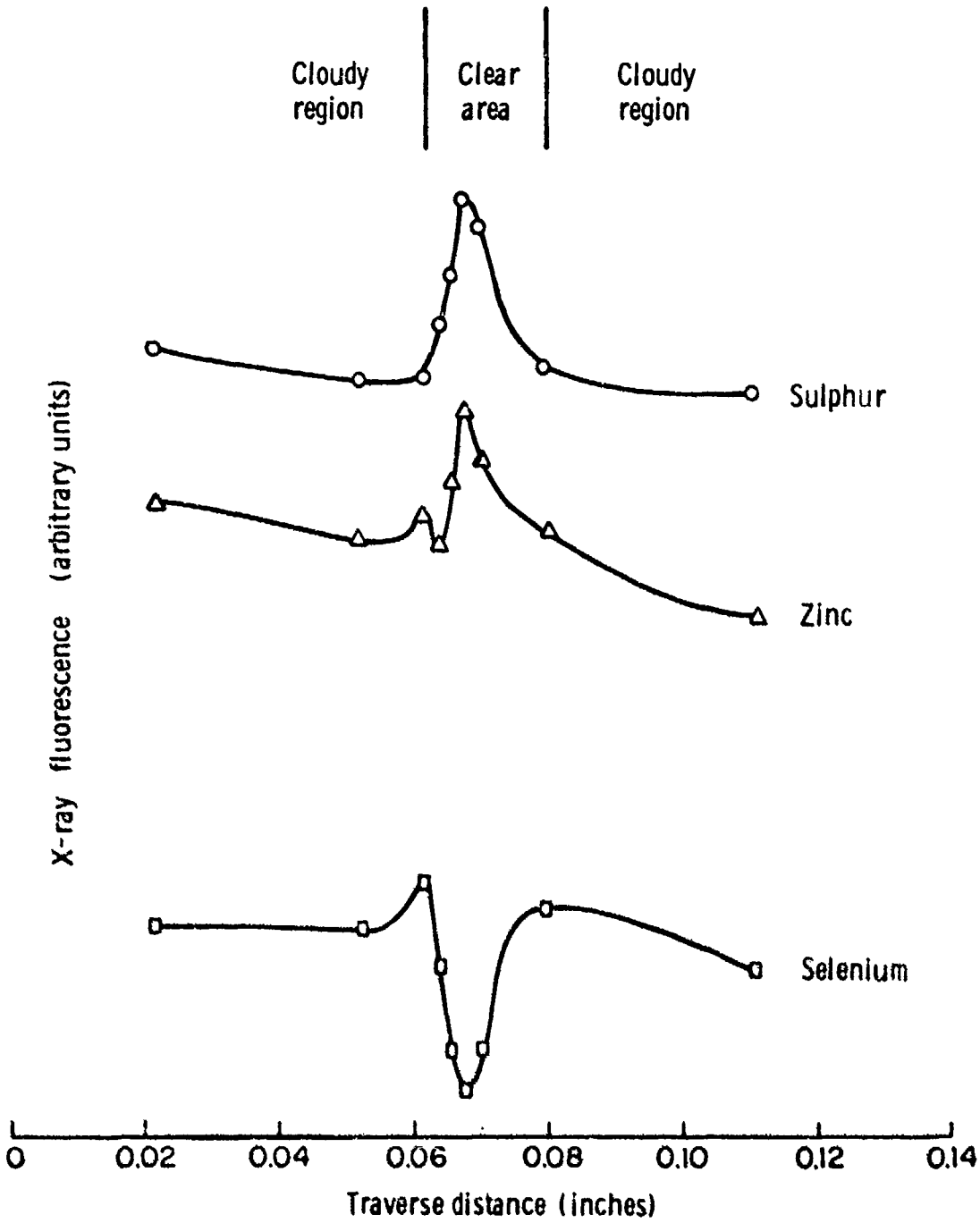

Figure 20. Microprobe Scan Through Clear and Cloudy Regions of Zinc Sulfo-Selenide Deposit.

regions of each phase. It is this latter situation which we felt might be occurring in the epitaxial deposition of cubic material onto hexagonal cores or dendrites resulting in the needle-like inclusions apparent in the microstructure.

Further support was given to this argument in SEM photographs taken on exaggerated nodules found in one of the deposits. Close examination of the nodules revealed needle-like protrusions growing out of the tip of each nodule (Figure 21a and b). At a higher magnification of these needles (Figure 22) one can observe the semblance of a hexagonal core approximately 0.5 μm in diameter, and the subsequent growth of more or less featureless knobs onto this core. These needle core sizes are comparable in size to the scatter sites estimated from the scatter analysis. In addition, the percent of the total volume taken up by the core area is not inconsistent with the estimates from X-ray diffraction analysis. It is our opinion, therefore, that a mixture of hexagonal and cubic phase is the major cause of scatter in these deposits. If this is the case, then scatter-free material can only be made by eliminating the hexagonal phase or by making all potential scatter sites small in relation to the wavelength of interest. The success we have achieved to date comes from our approaching this latter condition.

3.7 Scatter Analysis

We have previously discussed the relative optical quality of zinc sulfide deposits, emphasizing the differences in scatter in the 6000 Å to 25,000 Å wavelength region. In an attempt to obtain more information regarding the scattering particles or inhomogeneities the scatter contribution to attenuation of transmitted light was analyzed in some detail. This was done by analyzing the turbidity coefficient calculated from transmission data taken on a Carey spectrometer as a function of wavelength in the following way.

We related the turbidity coefficient to the observed transmission (power transmitted/ power incident) through the approximation

(a)

4000×

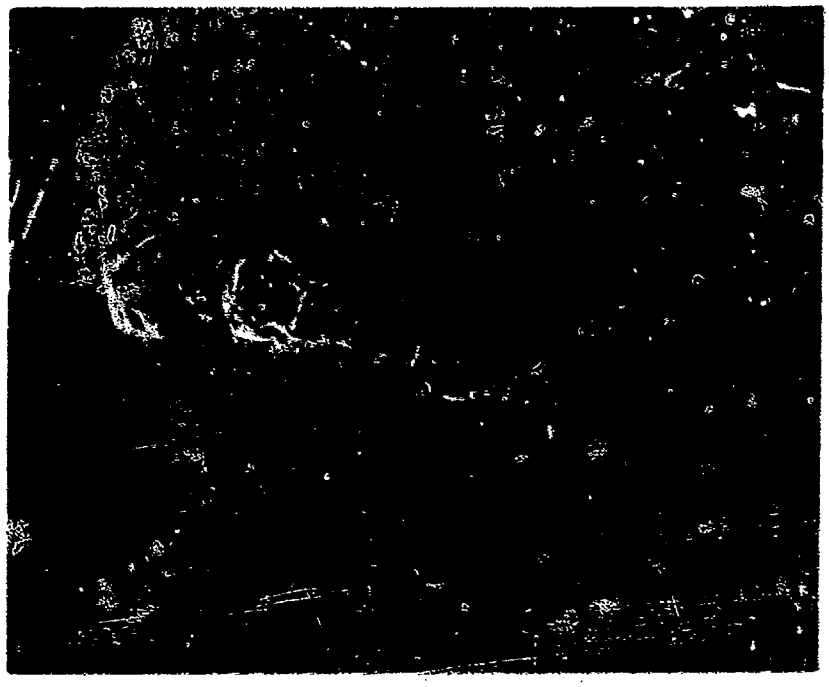

(b)

2000×

Figure 21. SEM Microphotographs of the Tips of Nodules From ZSS-33.

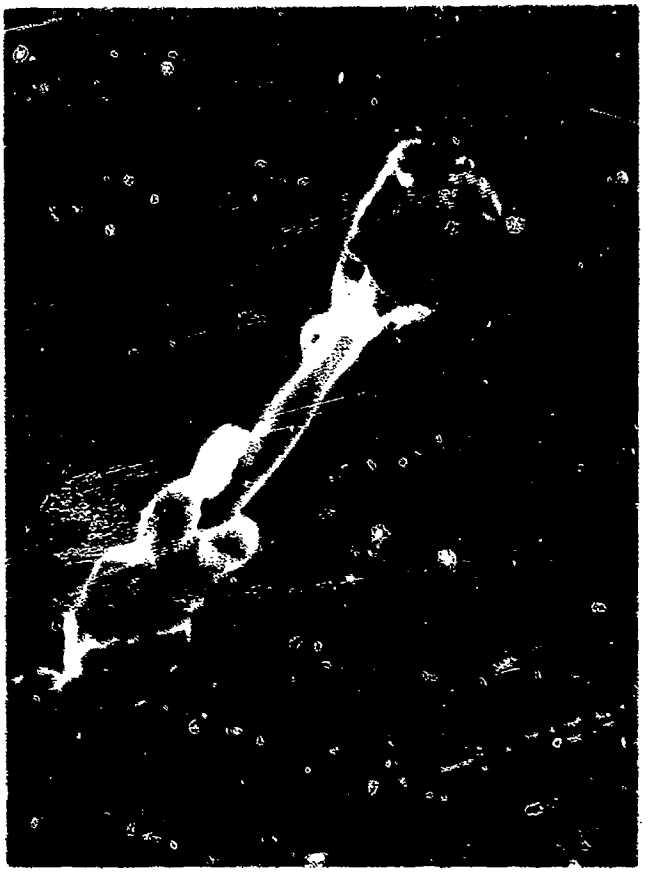

10,000×

Figure 22. Enlarged View of Needle on Tip of Nodule from ZSS-33 Showing Core and Subsequent Growth Onto the Core.

$$T = T_o \; e^{-\tau \ell}$$

where T is the transmission, τ the turbidity coefficient, ℓ the sample thickness, and T_o accounts for that part of the reduction in transmission arising from causes other than scattering. In general, the scattering will be wavelength dependent, so that τ will be a function of λ. On ther other hand, we will assume that T_o is essentially independent of λ.

A very significant factor in T_o is, of course, the Fresnel reflection at the sample surfaces. From this effect alone, $T_o = (1-R)/(1+R)$, where R is the one-surface reflectivity. Also contributing to T_o would be the effect of large opaque particles which would obscure transmission in a wavelength-independent manner.

Since $\tau\ell = -\ln (T/T_o)$, we may calculate values of τ from measured transmission as a function of wavelength for any assumed value of T_o. If we assume that the wavelength dependence of τ is given by $\tau = \text{const } \lambda^{-n}$, a plot of log τ vs log λ should result in a straight line of slope -n. Our approach then, is to determine by trial and error the value of T_o that produces values of τ which result in the best straight line on a log-log plot of τ vs λ. An example of such a plot is shown in Figure 23. Values of T_o and n determined for six (6) samples is shown in Table 11.

The purpose of analyzing the data in this manner is that it may be possible to attach a physical significance to the value of n obtained. Thus, in the familiar case of Rayleigh scattering for small particles (< 500 Å) at 1.06 μm one should obtain n = 4. On the other hand, large non-absorbing particles (from 2000 Å to 2 μm) having an index of refraction differing only slightly from that of the surrounding medium will produce a value of n = 2.[4]

What is gained from the "turbidity analysis" is relative information from run to run regarding size, shape, geometry, etc. of the scattering particles or inhomogeneities. For this purpose we make a few assumptions,

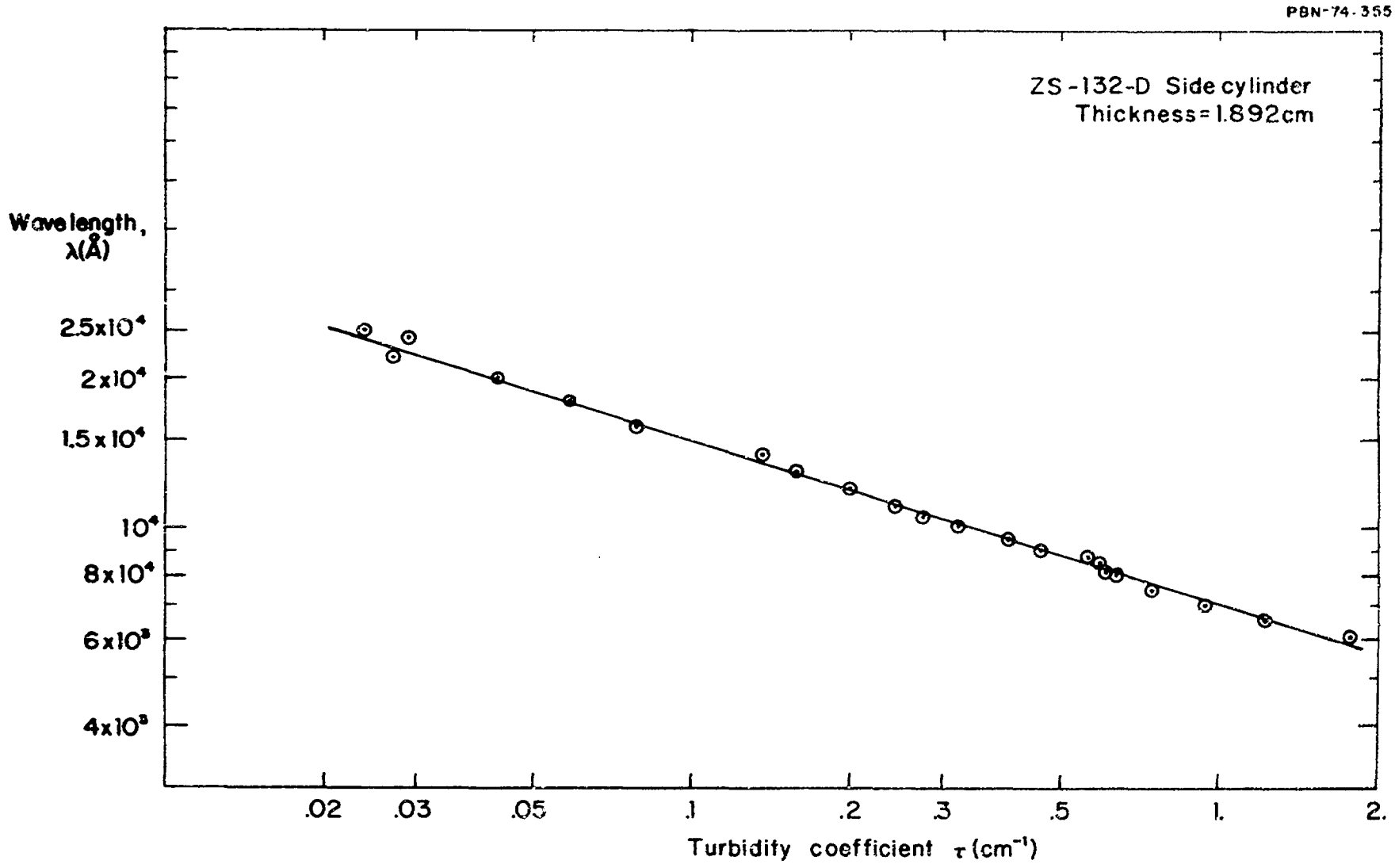

Figure 23. Representative log-log plot of calculated turbidity coefficient vs wavelength. T_o has been chosen to produce a straight line (see text).

TABLE 11

TURBIDITY ANALYSIS OF ZnS PLATE DEPOSITS

Sample	Thickness (cm)	T_o	n
ZS-132D Side Cylinder			
Parallel to growth direction	1.892	0.45	3.0
Parallel to growth direction	1.082	0.49	3.2
Normal to growth direction	1.062	0.53	4.0
ZS-130P Side 4			
Parallel to growth direction	1.123	0.68	2.5
45° from growth direction	1.041	0.67	2.9
Normal to growth direction	1.128	0.66	3.2

the first of which is that there is no absorption. We can then separate the observed transmission T into physical phenomena we speculate exist. The expression $T = T_o\ e^{-\tau \ell}$ can then be further broken down to:

$$T = T_R\ T_{OS}\ T_{OB}\ e^{-\tau_2 \lambda^{-2} \ell}\ e^{-\tau_4 \lambda^{-4} \ell}$$

where

T_R = reduction in transmitted intensity due to reflection
T_{OS} = reduction due to large surface obscurations
T_{OB} = reduction due to large bulk obscruations
τ_2 = a constant determined by the size, distribution, shape, and quantity of scatter sites having size 2000 Å to 2 μm and small index differences.
τ_4 = a constant determined by the size, distribution, shape and quantity of scatter sites having sizes less than 500 Å

By eliminating T_{OS} through proper surface polishing and T_{OB} by selecting samples with no visible inclusions such as zinc particles, we can approximate T_o by calculating reflection losses (T_R) using reported index of refraction data. The remaining attenuation should then fit either the λ^{-2} or λ^{-4} dependence as shown above. In actual trial cases the λ dependence appears to be a combination λ^{-2} and λ^{-4} dependence, and we interpret this as a distribution of both particle optical size ranges. That is, an intermediate value of n between 2 and 4 is interpreted as an approximate blend of both modes of scatter.

Looking at the data in Table 11 several things are immediately evident. The range of values of T_o means that there is considerable large particle obscuration in a number of the samples. It is also evident from the values of n that the scatter cross-section of the particles is measurably larger, looking parallel to the growth direction than normal to the growth direction. In the samples from ZS-130P a third direction, 45° from both the normal and parallel samples, was also measured and this sample showed an intermediate value of n indicating an intermediate particle cross-section size at that angle. This latter fact strongly suggests that the scatter particles are not spherical and

that they have a directional dependence. This is supported by the fact that almost all samples visually image much better through the cross-section than parallel to the growth direction. X-ray analysis of this same set of three samples from ZS-130P has been done to determine if there is a preferred growth direction or if directionally-dependent stacking faults exist. Step-scanning of the entire (111) peak parallel and normal to the growth direction does indeed show a slightly higher degree of stacking faults normal to the growth direction. All of this lends still further support to the argument that the observed scatter is due to index inhomogeneities caused by mixtures of the poly-type forms of ZnS.

4.0 CONCLUSIONS

The feasibility of using the CVD process to prepare high quality zinc sulfide hemispherical domes and plates for multispectral applications was established. A 9-inch diameter hemispherical dome and a 10 × 10 × 5/8-inch plate were fabricated with the requisite optical finish suitable for application at 1.06 μm and for the 8.0 to 11.5 μm spectral range. It was possible to image through both of these pieces of hardware in the visible range and the imaging quality was particularly impressive in the case of the hemispherical dome. The feasibility of multidome depositions was also established with the deposition of four (4) domes in one deposition run.

Considerable progress was also achieved in the further development of zinc sulfo-selenide solid solutions. The banding problem attributed to small compositional fluctuations was improved to a tolerable limit and undistorted imaging in the visible range was achieved through precise control of all process parameters. The addition of long wavelength transmission achieved with the zinc sulfo-selenide over pure zinc sulfide did not warrant the additional cost of the sulfo-selenide. Therefore, at the present time, pure zinc sulfide is judged a better multispectral window material candidate.

At present the optimum type of CVD zinc sulfide is deposited at 650° C in the presence of excess zinc vapor. These conditions yield a fine-grain size material that contains a minimum number of scatter sites. The major cause of scatter sites in zinc sulfide is the co-existence of both the hexagonal and cubic phases and that scattering from this mixture can best be avoided by generating a small grain size material. The small grain size also helps in the hardening of the window and enhances its enviromental endurance.

Feasibility was shown in the concept of using coatings to increase the durability of the CVD materials to in-flight environments. Coatings

can be applied and the apparent strength of the material can be increased as was shown in the flexural testing of several of the deposits. Additional work will have to be done, however, to determine if the coatings enhance the environmental durability of the base material.

5.0 REFERENCES

1. B. A. diBenedetto, J. Pappis, A. J. Capriulo, Technical Rpt. AFAL-TR-73-252, July 1973.

2. R. Gentilman, Ph. D. Thesis, M. I. T., Sept. 1973, pp. 35-55, 110-117.

3. R. Gentilman, J. Am. Ceram. Soc. 56 (1973) 623.

4. H. C. Van de Hulst, "Light Scattering by Small Particles," J. Wiley and Sons, New York, 1957, p. 133.

☆U.S.Government Printing Office: 1975 – 657-023/729